

## Accepted Manuscript

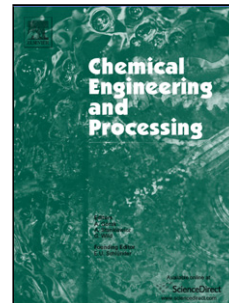
Title: A hydrodynamic model for biomass gasification in a circulating fluidized bed riser

Authors: Mohamed I. Hassan, Yassir T. Makkawi

PII: S0255-2701(18)30273-3  
DOI: <https://doi.org/10.1016/j.cep.2018.05.012>  
Reference: CEP 7290

To appear in: *Chemical Engineering and Processing*

Received date: 3-3-2018  
Revised date: 18-5-2018  
Accepted date: 22-5-2018



Please cite this article as: Hassan MI, Makkawi YT, A hydrodynamic model for biomass gasification in a circulating fluidized bed riser, *Chemical Engineering and Processing - Process Intensification* (2018), <https://doi.org/10.1016/j.cep.2018.05.012>

This is a PDF file of an unedited manuscript that has been accepted for publication. As a service to our customers we are providing this early version of the manuscript. The manuscript will undergo copyediting, typesetting, and review of the resulting proof before it is published in its final form. Please note that during the production process errors may be discovered which could affect the content, and all legal disclaimers that apply to the journal pertain.

# **A hydrodynamic model for biomass gasification in a circulating fluidized bed riser**

Mohamed I Hassan <sup>a,1</sup> and Yassir T Makkawi <sup>b,\*</sup>

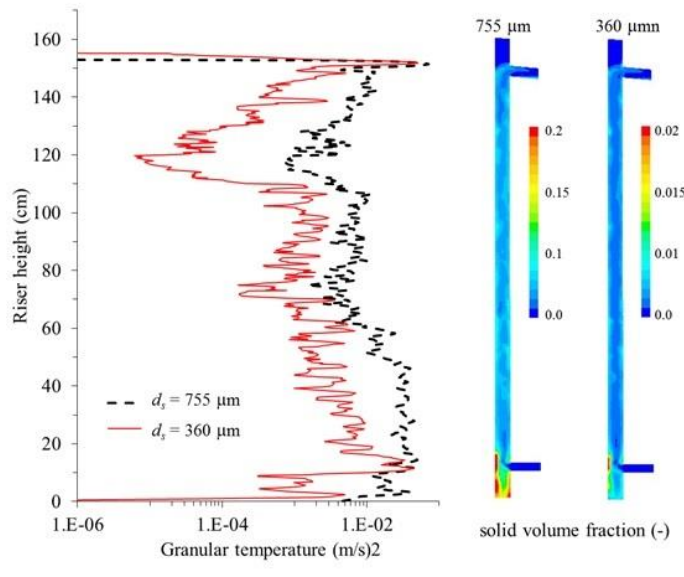
<sup>a</sup> European Bioenergy Research Institute (EBRI), School of Engineering and Applied Science, Aston University, Birmingham B4 7ET, UK

<sup>b</sup> Chemical Engineering Department, College of Engineering, American University of Sharjah, P.O. Box 26666, Sharjah, United Arab Emirates.

<sup>1</sup> Current address: Chemical Engineering Department, Faculty of Engineering, Jazan University, P.O. Box 114, Jazan, KSA. E-mail address: [mihassan@jazanu.edu.sa](mailto:mihassan@jazanu.edu.sa)

\* Corresponding author: Tel.: +97165152167; fax: +97165152979. E-mail address: [ymakkawi@aus.edu](mailto:ymakkawi@aus.edu) (Yassir T. Makkawi).

## Graphical abstract



## Highlights

- Hydrodynamic model of a binary solid mixture in a CFB riser is presented.
- Constitutive equations and alternative solution methods have been assessed.
- The model has been validated against experimental particle tracing and pressure measurements.
- The model proved to be robust and accurate, hence, highly recommended for the simulation of biomass gasification in a CFB riser.
- 

## Abstract

This study presents a three-dimensional Computational Fluid Dynamic (CFD) model and experimental measurements of the hydrodynamics in the riser section of a Circulating Fluidized Bed (CFB) biomass gasifier consisting of a binary mixture of polydisperse particles. The model is based on multi-fluid (Eulerian-Eulerian) approach with constitutive equations adopted from the Kinetic Theory of Granular Flow (KTGF). The study first presents an assessment of the various options of the constitutive and closure equations for a binary mixture followed by sensitivity analysis of the model to the solution time step, cell size, turbulence and the alternative formulations

of the granular energy equation. Accordingly, a robust and reliable hydrodynamic model is recommended and validated using conventional pressure measurements and Positron Emission Particle Tracking (PEPT) technique. Furthermore, the model predictions and experiments revealed evidence of the particle re-circulation within the lower part of the riser, which is an important feature contributing to rapid mass and heat transfer in a CFB gasifier. The present hydrodynamic model can be further developed; by incorporating appropriate reactions and heat transfer equations, in order to fully predict the performance and products of a CFB biomass gasifier.

*Keywords: Circulating fluidized bed; CFD modeling; hydrodynamics; Experiment validation; Gasification*

<b>Nomenclature</b>	
$\bar{I}$	unit tensor (-)
$C_d$	particle drag coefficient (-)
$C_{fr}$	Friction coefficient (-)
$C_1, C_2, C_3$	turbulence model constants (-)
$d_i$	diameter of solid phase $i$ (m)
$e$	particle restitution coefficient (-)
$g_0$	radial distribution function (-)
$G_k, G_b$	turbulence kinetics due to velocity gradient and buoyancy, respectively
$\vec{g}$	gravity ( $\text{m s}^{-2}$ )
$K$	solid-solid momentum exchange coefficient ( $\text{kg m}^{-3} \text{s}^{-1}$ )
$k_e$	turbulence kinetic energy ( $\text{m}^2 \text{s}^{-2}$ )
$w_t$	turbulence dissipation energy ( $\text{m}^2 \text{s}^{-3}$ )
$\sigma_e, \sigma_t$	prandtl numbers for kinetic and dissipation energies, respectively (-)
$N_c$	Courant number (-)
$P$	pressure (Pa)
$Re$	Reynolds number (-)
$t$	time (s)
$\vec{u}_g, \vec{u}_s$	gas and solid velocity vector ( $\text{m s}^{-1}$ )
$u_r$	particle terminal velocity ( $\text{m s}^{-1}$ )
<b>Greek letters</b>	
$\varepsilon$	volume fraction (-)

$\beta$	momentum exchange coefficient ( $\text{kg m}^{-3} \text{s}^{-1}$ )
$\gamma$	collisional energy dissipation ( $\text{kg m}^{-1} \text{s}^{-3}$ )
$\theta$	granular temperature of solid phase $i$ ( $\text{m}^2 \text{s}^{-2}$ )
$k$	diffusion coefficient of granular energy ( $\text{kg m}^{-1} \text{s}^{-1}$ )
$\phi'$	specularity coefficient (-)
$\rho$	density ( $\text{kg m}^{-3}$ )
$\mu_{eff}$	effective turbulence viscosity ( $\text{kg m}^{-1} \text{s}^{-1}$ )
$\bar{\bar{\tau}}$	shear stress tensor ( $\text{kg m}^{-1} \text{s}^{-2}$ )
$\Delta_{cell}$	computational face cell size (m)
<b>Subscripts</b>	
$s, g$	solid and gas phases, respectively
$w$	wall
$col$	wall
$kin$	kinetic

## 1. Introduction

The application of Circulating Fluidized Beds (CFB) to biomass thermal conversion (gasification and pyrolysis) is currently receiving increasing attention due to its good mixing, high thermal efficiency and most importantly, its excellent scale-up potentials up to around 1000 tonnes of dry biomass feed per day.<sup>1</sup> However, practical experimental investigation in a CFB, for testing new feedstock or parametric sensitivity analysis, is often difficult, expensive and requires high expertise due to the complexity associated with the high-temperature operation and release of particulate and toxic/highly flammable gases. Computational Fluid Dynamic (CFD) models integrated with equations describing the heat transfer, transport of species and chemical reactions, offers an alternative solution. Such models can be solved using standard computers at a reasonable

computational time to reveal detailed features of the reactor such as the solid and gas distribution, velocities, pressure, temperature, gas species concentrations and product quality. As a result, studies using CFD models for the simulation and analysis of processes involving rapid thermochemical conversion, such as in catalytic reforming of gases, combustion of solid waste and conversion of biomass to bio-fuels are nowadays frequently reported in the literature.<sup>2,3</sup> The advances in computational power has also been matched with the development of user-friendly commercial software. Examples of some of the widely used commercial software for particle-gas flow simulation are ANSYS (FLUENT and CFX), COMSOL and Barracuda. Other highly functional open-source CFD software is also available free for academic use such as MFIX and OpenFoam. Most of these codes offer the solution of multiphase flows in Eulerian-Eulerian or Eulerian-lagrangian approaches. The latter, which is also referred to as Eulerian-DEM, has the advantage of being more accurate by tracking each individual particle, but at the expense of high computational time (CPU time). The former treats both of the solid and gas phases as an interpenetrating continuum based on ensemble averaging, hence relatively faster in handling large systems but less revealing at the discrete particle level. Nevertheless, the Eulerian-Eulerian approach remains the most popular option among academic researchers for the simulation of multiphase flow with chemical reactions. Having said that, it must be noted that applying the Eulerian-Eulerian approach to three-dimensional simulations of polydispersed suspension requires a good understanding of the various constitutive and closure equations in addition to careful setting of the solution procedure.

As noted above, one of the major attractive features of the CFB gasification technology is its high thermal efficiency; it allows for the supply of the heat required to derive a highly endothermic

thermochemical conversion process in a closed loop without the need of external heating. For example, in steam gasification (also referred to as pyrolytic gasification), this is achieved by coupling two reactors, creating what is usually referred to as dual fluidized bed (DFB) gasifier. In this arrangement, one reactor is used for the gasification and another is used for the char combustion. In the gasifier, the biomass is brought into contact with the fluidizing gas (steam or air/steam mixture) and a heat carrier solid, ideally to maintain the gasifier within the range of 750–950 °C<sup>2,4</sup>. In the combustor, the transferable heat carrier solid (such as sand) is raised to a high temperature by char combustion. The use of steam in biomass gasification is particularly attractive as it enhances hydrogen production through a water gas shift reaction.<sup>5,6</sup> Fig. 1 shows two examples of the arrangements of a DFB reactor for biomass steam gasification. In this study, the focus is made on the simulation of the riser, shown in the left section of the CFB arrangement given in Fig. 1-b. Here, the gasification is carried out in the riser and the reaction is entirely driven by hot circulating inert solid introduced at the bottom of the riser from the connected combustor.

Review of the recent literature on modeling of biomass gasification in fluidized bed reactors show that the CFB type received less attention compared to the bubbling bed. See Table 1 for examples of the most recent studies. Modeling of the flow hydrodynamics in a CFB gasifier is challenging due to the existence of multi-solids which undergo complex collisional interactions while dispersing in a continuum gas phase. Furthermore, the accuracy of the Eulerian-Eulerian model for a polydispersed suspension is heavily dependent on a range of constitutive and closure equations, as noted earlier. Therefore, the overall objective of this study is to identify a reliable and robust hydrodynamic model, which can be used as a platform for further development of a full predictive tool of biomass gasification in a CFB riser.

The model is solved using ANSYS FLUENT commercial CFD code. This code has the advantage of providing a range of built-in functions and options that allow for the assessment of the various constitutive equation and solution procedures, as well as providing UDF access to the code solver. The hydrodynamic predictions are validated with experimental data obtained in a cold flow CFB riser using pressure measurements and positron emission particle tracking (PEPT).

## 2. Experiments

Experiments in a cold flow CFB (isothermal and non-reactive) have been carried out for two purposes. First, to collect data for the validation and assessment of the hydrodynamic model and its constitutive equations. Second, to visually observe the flow characteristics and establish a rough estimate of the range of operating condition for future simulation of biomass gasification in a CFB riser. The set-up shown in Fig. 2 mainly comprises a relatively short riser with aspect ratio (height/diameter)=32.6, downer section, two cyclones, solid receiving tank and a data acquisition system. The dimensions of the riser were carefully selected to allow covering the range of flow regimes commonly observed in a biomass gasifier (i.e. dense bottom and rapid dilute suspension at the top). The riser is made of glass and fitted with eight pressure probes connected to piezoresistive pressure sensors/transmitters. The downer side was equipped with an inlet for auxiliary air and a diversion valve to allow measuring the total solid circulation rate. Two rotameters were used to measure the airflow required to fluidize the bed and maintain the solid circulation. In order to resemble the particulate in a biomass gasifier, a mixture of sand and wood particles (Geldart group B particles) is used as the bed material. In some cases, narrow-sized glass bead mixtures were used instead of sand, either as a mixture with wood or as a single solid phase.

Tables 2 gives the details of the equipment, material and range of operating condition considered in the experiments.

### **2.1. Pressure measurements**

The axial pressure profile in the riser was measured using eight pressure sensors/transmitters (Range: 1–70 mbar; model: CTEM70070GY4) connected to probes inserted at various heights above the gas distributor (21 cm, 33 cm, 45 cm, 76 cm, 107 cm and 138 cm), as shown in Fig. 2. The lower probes were distributed at short distances in order to capture the steep variations in pressure in this region. The tips of the probes were covered by a fine metal mesh to prevent the particles from entering the probes. A data acquisition system was used to record the pressure at the rate of 1 Hz. The pressure at each point was calculated using localized data averaged over 5–10 minutes of continuous and steady circulation.

### **2.2. Particle tracking**

Positron Emission Particle Tracking (PEPT) is a non-invasive technique that allows tracking the motion of a single radioactively labeled tracer particle within a multiphase flow. The principle of the PEPT technique and its application in studying particle dynamics can be found in the open literature.<sup>14–17</sup> The facility used in this study was located at the University of Birmingham, Nuclear Physics Research Center. Prior to fluidization experiment, a single tracer particle was activated with Fluorine-18 and placed inside the CFB solid receiving tank. The activated particle was then tracked during circulation using Gamma photons detector plates located around the lower part of the CFB riser, as shown in Fig. 3. The experiments were conducted using a bed material consisting

of sand–wood mixture. Two sets of data were produced; one with the system tracking an activated wood particle and another with an activated sand particle.

The recorded data were analyzed using MATLAB software to obtain transient and time-averaged information on the particle velocity and location within the PEPT detection zone. Because the radioactive particle was circulating between the riser and downer side, there was few minutes delay between each set of detections, as will be demonstrated later. The total duration time used for the collection of the data was around 2 hours, beyond this time, the activity of the particles decays rapidly. All the measurements were taken at one fixed level within the lower part of the CFB riser due to difficulty in moving the sensors to higher levels (see Fig. 3b).

### 3. Hydrodynamic model equations

The mathematical model used to simulate the CFB riser hydrodynamics is described below. The

multiphase flow mixture in the riser is assumed to consist of a polydispersed binary solid mixture and air as the fluidizing agent.

#### 3.1. Main model equations

The main transient model equations include continuity, momentum and granular energy in addition to turbulence closure equations. The Continuity equations are given by:

$$\frac{\partial(\varepsilon_g \rho_g)}{\partial t} + \nabla(\varepsilon_g \rho_g \vec{u}_g) = 0 \quad (1)$$

$$\frac{\partial(\varepsilon_{s_i} \rho_{s_i})}{\partial t} + \nabla(\varepsilon_{s_i} \rho_{s_i} \vec{u}_{s_i}) = 0 \quad i = 1 \text{ or } 2 \quad (2)$$

$$\sum_{i=1}^2 \varepsilon_{s_i} + \varepsilon_g = 1 \quad (3)$$

where  $\varepsilon$  is the volume fraction,  $\rho$  is the density,  $\vec{u}$  is the velocity vector. The subscripts  $g$  and  $s$  stand for the air and solid phases, respectively, while  $i = 1$  or  $2$  refers to any of the two solid phases. Note that the right side of Eqs 1 and 2 is zero because no mass transfer takes place (isothermal and non-reactive system).

The momentum equations are given by:

$$\frac{\partial(\varepsilon_g \rho_g \vec{u}_g)}{\partial t} + \nabla(\varepsilon_g \rho_g \vec{u}_g \vec{u}_g) = -\varepsilon_g \nabla P_g + \nabla \bar{\bar{\tau}}_g - \sum_{j=1}^2 \beta_{g-si} (\vec{u}_g - \vec{u}_{sj}) + \varepsilon_g \rho_g \vec{g} \quad (4)$$

$$\begin{aligned} \frac{\partial(\varepsilon_{si} \rho_{si} \vec{u}_{si})}{\partial t} + \nabla(\varepsilon_{si} \rho_{si} \vec{u}_{si} \vec{u}_{si}) = \\ \varepsilon_{si} \nabla P_g - \nabla P_{si} + \nabla \bar{\bar{\tau}}_{si} + \beta_{g-si} (\vec{u}_g - \vec{u}_{si}) + K_{ij} (\vec{u}_{si} - \vec{u}_{sj}) + \varepsilon_{si} \rho_{si} \vec{g} \quad i \text{ and } j = 1 \text{ or } 2 \end{aligned} \quad (5)$$

where  $\beta$  and  $K$  are the solid-gas and solid-solid momentum exchange coefficient, respectively.  $P$ ,  $\bar{\bar{\tau}}$  and  $\vec{g}$  are the solid pressure, solid shear stress tensor and gravity constant, respectively.

The energy equation, derived from the principles of the Kinetic Theory of Granular Flow (KTGF)<sup>18-20</sup> is used to calculate the granular temperature, an important parameter for calculating the particles interaction and the energy lost during. This is given by the following pseudo-thermal energy balance equation:<sup>18-20</sup>

$$\begin{aligned} \frac{2}{3} \left[ \frac{\partial}{\partial t} (\varepsilon_{si} \rho_{si} \theta_{si} + \nabla \cdot (\varepsilon_{si} \rho_{si} \vec{u}_{si} \theta_{si})) \right] = (-P_{si} \bar{\bar{I}} + \bar{\bar{\tau}}_{si}) : \nabla \vec{u}_{si} + \nabla \cdot (k_{si} \nabla \theta_{si}) - \gamma_{si} - 3\beta_{si} \theta_{si} \\ i = 1 \text{ or } 2 \end{aligned} \quad (6)$$

where  $\theta$ ,  $k$  and  $\gamma$  represent the granular temperature, diffusion coefficient and collisional dissipation of energy. The last term on the right side represents the energy exchange between the solid phase  $i$  and the fluid. Eq. 6 can be reduced to an algebraic expression by neglecting the convection and diffusion terms to give the following equation:<sup>21</sup>

$$0 = (-P_{si}\bar{l} + \bar{\tau}_{si}) : \nabla \vec{u}_{si} - \gamma_{si} - 3\beta_{si}\theta_{si} \quad i = 1 \text{ or } 2 \quad (7)$$

The validity of this simplified equation for the case under consideration will be discussed in the results section.

### 3.2. Constitutive and closure equations

Constitutive equations for the Eulerian two-phase flow model are widely reviewed and validated for the case of a monodispersed dense-intermediate suspension<sup>22-29</sup>. In particular, the solid-gas momentum exchange equation (gas drag law) for bubbling fluidized beds received the most attention<sup>26-28</sup>. However, less attention has been given to the case of polydispersed dilute suspension, such as in CFB systems. In this section, the focus is made on the constitutive and closure equation describing the solid-gas and solid-solid momentum exchange, radial distribution function, solid pressure and turbulence. The remaining constitutive and closure equations, which are used as default, are given in Table 4 as part of the final recommended constitutive and closure equations.

#### 3.2.1. Solid-gas and solid-solid momentum exchange coefficients

Multiphase flow in a CFB riser generally falls under the category of rapid particle motion. However, the bottom of the riser exhibits a relatively dense flow structure that gradually decreases to form a rapid dilute flow toward the exit. It is also recognized that the major heat and mass transfer in a CFB gasifier take place in the bottom part of the riser. Therefore, it is important to apply a solid-gas drag equation capable of capturing such variations in the flow regime. Here, the two most widely used models, reported to satisfy this requirement, will be used and their capabilities in correctly predicting dilute binary mixture hydrodynamics will be assessed by

comparing with experimental measurements. Gidaspow<sup>30</sup> derived the following drag law by combining Ergun<sup>31</sup> correlation for packed bed with Wen and Yu<sup>32</sup> correlation for a dilute flow as follows:

$$\beta_{si} = \frac{3}{4} C_d \frac{\varepsilon_{si} \varepsilon_g \rho_g |u_{si} - u_g|}{d_{si}} \varepsilon_g^{-2.65} \quad \text{if } \varepsilon_g > 0.8 \quad (8)$$

$$\beta_{si} = 150 \frac{\varepsilon_{si}(1-\varepsilon_g)\mu_g}{\varepsilon_g d_{si}^2} + 1.75 \frac{\varepsilon_{si} \rho_g |u_{si} - u_g|}{d_{si}} \quad \text{if } \varepsilon_g \leq 0.8 \quad (9)$$

where  $C_D$  is the single particle drag coefficient given by:

$$C_D = \frac{24}{\varepsilon_g Re} \left[ 1 + 0.15(\varepsilon_g Re)^{0.687} \right] \quad \text{if } \varepsilon_{si} Re \leq 1000 \quad (10)$$

$$C_D = 0.44 \quad \text{if } \varepsilon_{si} Re \geq 1000 \quad (11)$$

Syamlal et al.<sup>33</sup> reported another formula described to be applicable to a wide range of solid concentration as follows:

$$\beta_{si} = \frac{3\varepsilon_{si}\varepsilon_g\rho_g}{4u_{r,si}^2 d_{si}} C_D \left( \frac{Re}{u_{r,si}} \right) |u_{si} - u_g| \quad i = 1 \text{ or } 2 \quad (12)$$

where  $u_{r,si}$  and  $C_D$  are the terminal velocity and single particle gas drag coefficients, respectively (detailed in Table 4). In the rest of this study, Eq. 12 will be used as default unless otherwise stated.

Compared to the gas-solid drag, the momentum exchange between the solid-solid in polydispersed mixtures is less understood and often neglected in the modeling of dilute suspension. This force, which arises from the velocity difference between the interacting solids, becomes important when the particles are significantly different in size and/or density, such as in the case of sand and biomass in gasification reactors. It is also crucially important in modeling segregation and mixing in dense bubbling fluidized beds.<sup>34</sup> In this study, the solid-solid momentum exchange coefficient is incorporated in the model by using the equation proposed by Syamlal<sup>35</sup> as follows:

$$K_{ij} = \frac{3(1+e_{ij})\left(\frac{\pi}{2} + \frac{\pi^2}{8} C_{fr,ij}\right) \rho_{si} \rho_{sj} \varepsilon_{si} \varepsilon_{sj} (d_{si} + d_{sj})^2 g_{0,ij}}{2\pi(\rho_{si} d_{si}^3 + \rho_{sj} d_{sj}^3)} (u_{si} - u_{sj}) \quad i \text{ and } j = 1 \text{ or } 2 \quad (13)$$

where  $C_{fr,ls}$  is the coefficient of friction between the two solid phases (assumed zero in this study due to the dilute nature of the flow),  $g_0$  is the radial distribution function (discussed in details in Section 3.2.2) and  $e$  is the particle restitution coefficient (given in Table 3). The subscripts  $i$  and  $j$  represent the two solid phases given that  $i \neq j$ .

### 3.2.2. Radial distribution function

The KTGF is based on the assumption that particles collision obeys Chapman-Enskog theory for molecules interactions in dense gases,<sup>36</sup> but with the granules exhibiting loss of momentum due to inelasticity. The probability of collisions are introduced in the Eulerian-Eulerian model through the radial distribution function,  $g_0$ , which appears in a number of the KTGF constitutive equations such as the solid pressure, the solid-solid momentum exchange and the solid shear viscosity. The majority of literature discussing the radial distribution function has been related to dense collisional flow, such as in bubbling fluidized beds.<sup>37-40</sup> The extent of its influence to dilute suspension, such as in a CFB, is less understood and is certainly worth investigating.

The most widely used radial distribution function for a monodispersed suspension is the one originally proposed by Bagnold<sup>41</sup> and later applied by Lun et al.<sup>19</sup> and Savage<sup>39</sup> as follows:

$$g_0 = \left[ 1 - \left( \frac{\varepsilon_s}{\varepsilon_{s,max}} \right)^{1/3} \right]^{-1} \quad (14)$$

where  $\varepsilon_{s,max}$  is the maximum allowable solid volume fraction, or packing limit. For the case of a binary solid mixture, the radial distribution is given by:

$$g_{0,ij} = \frac{g_{0i}d_{si} + g_{0j}d_{sj}}{d_{si} + d_{sj}} \quad i \text{ and } j = 1 \text{ or } 2 \quad (15)$$

where  $g_{0,i}$  is for a selected solid phase  $i$  taking into account the effect of its own class in addition to the effect of the other particle. This is given by a modified Bagnold function as follows:<sup>21</sup>

$$g_{0i} = \left[ 1 - \left( \frac{\varepsilon_{s,all}}{\varepsilon_{s,max}} \right)^{1/3} \right]^{-1} + \frac{1}{2} d_{si} \sum_{j=1}^2 \frac{\varepsilon_{sj}}{d_{sj}} \quad i \text{ and } j = 1 \text{ or } 2 \quad (16)$$

The maximum allowable solid volume fraction in a binary mixture,  $\varepsilon_{s,max}$ , is calculated by using the values of maximum packing for each solid phase.<sup>19,21,42</sup> The total solid volume fraction,  $\varepsilon_{s,all}$ , is obtained by the summation of the volume fraction of the two solid phases.

Iddir and Arastoopour<sup>43</sup> proposed an alternative formula of  $g_0$  which reduces to the following simplified form:

$$g_{0,i} = \frac{1}{\left( 1 - \frac{\varepsilon_{s,all}}{\varepsilon_{s,max}} \right)} + \frac{3}{2} d_{si} \sum_{j=1}^2 \frac{\varepsilon_{sj}}{d_{sj}} \quad i \text{ and } j = 1 \text{ or } 2 \quad (17)$$

A similar formula for multi-solids was derived by Lebowitz<sup>44</sup> and used by Syamlal<sup>33</sup> for a binary mixture as follows:

$$g_{0,ij} = \frac{1}{\varepsilon_g} + \frac{3d_{si}d_{sj}}{\varepsilon_g^2(d_{si} + d_{sj})} \sum_{k=1}^2 \frac{\varepsilon_{sk}}{d_{sk}} \quad i \text{ and } j = 1 \text{ or } 2 \quad (18)$$

which reduces to the following formula for a selected solid phase  $i$ :

$$g_{0,i} = \frac{1}{\varepsilon_g} + \frac{3d_{si}}{2\varepsilon_g^2} \sum_{k=1}^2 \frac{\varepsilon_{sk}}{d_{sk}} \quad i = 1 \text{ or } 2 \quad (19)$$

where  $\varepsilon_g$  is the void fraction given by:

$$\varepsilon_g = 1 - \sum_j^2 \varepsilon_{sj} \quad (20)$$

It is worth noting that, in most of the currently available radial distribution functions, including the ones above, it is assumed that the function is independent of the particle density. However, there is an argument that such assumption may not be accurate, especially if the densities are considerably different. Wang et al.<sup>38</sup> derived a modified radial distribution function including the particle densities using data from discrete hard-sphere model simulation. The modified function produced accurate results, however, within the low range of particle volume fraction ( $<0.2$ ), the effect of density was clearly negligible. It was also shown that the computed results from Syamlal's formula (Eq. 8) are in good match with the simulation.

### 3.2.3. Solid pressure

The solid pressure is a measure of the momentum transfer due to the streaming motion of the particles. It is an important parameter involved in the solution of the solid phase momentum and kinetic energy equations (Eqs. 5 and 6, respectively). The widely used solid pressure equation for the simple case of a monodispersed suspension was derived from the principle of the KTGF and is given by the following equation:<sup>19</sup>

$$P_s = \varepsilon_s \rho_s \theta_s + 2\rho_s(1 + e_s)\varepsilon_s^2 g_0 \theta_s \quad (21)$$

where the first term in the right side represents the kinetic contribution arising from the momentum transfer due to the solid movement across a shear layer and the second term represents the collisional contribution arising from the direct solid-solid contacts. For a dilute suspension, it is suggested that the collisional term could be neglected as its contribution to the total solid pressure becomes small.<sup>33</sup> However, for the solid concentration within the range of  $< 0.2$ , calculations have shown that the kinetic and collisional contributions are equally important<sup>29</sup>, hence, both terms are

retained in this study to ensure applicability of the solid pressure equation to the range of solid concentration commonly observed in CFB risers.

For the case of a binary mixture, Gidaspow<sup>30</sup> modified Eq 21 to take care of the existence of two different particles by adding up the collisions. Accordingly, the solid pressure for a selected solid phase  $i$  in a binary mixture is given by:

$$P_{si} = \varepsilon_{si}\rho_{si}\theta_{si} + 2\varepsilon_{si}\rho_{si}\theta_{si} \sum_{j=1}^2 \left[ \frac{(d_{si}+d_{sj})}{2d_{si}} \right]^3 (1 + e_{s,ij})g_{0,ij}\varepsilon_{s,ij} \quad i = 1 \text{ or } 2 \quad (22)$$

where  $\theta_{si}$  is the granular temperature of the solid phase  $i$ .

#### 3.2.4. Turbulence

The CFB hydrodynamics is expected to be affected by the swirl and rotation, depending on the magnitude of the mean flow Reynolds number. In this study, the dispersed RNG  $k$ - $\varepsilon$  model has been used to assess the model sensitivity to such effects. Compared to other optional turbulence models available in FLUENT, the dispersed RNG  $k$ - $\varepsilon$  model is described to be more accurate and reliable for a wider class of flows.<sup>21</sup> The model involves the solution of two equations calculating the turbulence kinetic energy,  $ke_t$ , and its dissipation,  $\omega_t$ , as follows:

$$\frac{\partial}{\partial t} (\rho_g ke_t) + \nabla(\rho_g ke_t u_g) = \nabla(\sigma_k \mu_{eff} \nabla ke_t) + G_k + G_b - \rho_g \omega_t - Y_M \quad (23)$$

$$\frac{\partial}{\partial t} (\rho_g \omega_t) + \nabla(\rho_g \omega_t u_g) = \nabla(\sigma_\omega \mu_{eff} \nabla \omega_t) + C_1 \frac{\omega_t}{ke_t} (G_k + C_3 G_b) - C_2 \rho_g \frac{\omega_t^2}{ke_t} \quad (24)$$

where  $G_k$  and  $G_b$  represent the generation of turbulence kinetic energy due to the velocity gradients and buoyancy, respectively.  $Y_M$  represents the contribution of the fluctuating dilatation incompressible turbulence to the overall dissipation rate.  $C_1$ ,  $C_2$ , and  $C_3$  are constants (values given in Table 3).  $\sigma_k$  and  $\sigma_\omega$  are the turbulence Prandtl numbers for  $ke_t$  and  $\omega_t$ , respectively.

The details of calculating the effective turbulence viscosity,  $\mu_{eff}$ , and other parameters of the RNG  $k-\varepsilon$  model can be found in ANSYS FLUENT documentarian.<sup>21</sup> The model sensitivity to the turbulence and comparison with the laminar flow assumption will be discussed in the result section.

#### **4. Simulation geometry, meshing and solution procedure**

The simulation geometry and domain is shown in Fig. 4. In defining the mesh size, the rule of thumb for a monodispersed solid mixture suggests a minimum cell face size of around 10 times the particle diameter. Applying this to a binary mixture, then the face cell size would be 10 times the larger size as an upper limit and 10 times the smaller particle as a lower limit. This is used as guide for initial set of the mesh size, however, because the computational time and solution accuracy are both critically dependent on the number of cells, sensitivity analysis deemed necessary in order to optimize the solution procedure and avoid the risk of losing relevant flow structures of any of the two particles in the mixture. ANSYS Workbench software was used to generate the final simulation geometry and meshes based on the specified minimum and maximum cell face sizes. The tetrahedral meshing function, available as one of the options in the software, was used to generate an unstructured element of different sizes and shapes depending on the element position.

In setting the solution time step, it is important to avoid instability, solution stiffness, and unrealistic long computational time, especially for a complex reactive system, such as the case considered here. It is generally understood that the stiffness and instability in solving the partial differential equations (PDEs) can be avoided by adopting a suitable time step and discretization scheme. The main model PDEs given in Section 3.1 were discretized using the first order upwind

implicit method. To control the update of computed variables at each iteration, the under-relaxation factors for the pressure and momentum were set to 0.2 and 0.5, respectively. In setting the step size, the following simple rule of thumb was used:

$$N_c = u_g \frac{\Delta t}{\Delta_{cell}} \quad i = 1 \text{ or } 2 \quad (25)$$

where  $N_c$ ,  $\Delta_{cell}$ ,  $\Delta t$  and  $u_g$  are the Courant number, cell face size and the vertical component of the gas velocity, respectively. For a monodispersed mixture, Cornelissen et al.<sup>45</sup> recommended a Courant number within the range of 0.03–0.3 while Gobin et al.<sup>46</sup> recommended the maximum value of 0.3. For a polydispersed mixture, Coroneo et al.<sup>47</sup> suggested that a Courant number within the range of 0.028–0.15 always gives an error below 10%. However, it has to be noted that generalization of such values should be treated with caution since the Courant number strongly depends on the particle sizes used. Nevertheless, if assuming the range given by Coroneo et al.<sup>47</sup> is the most appropriate (they used particles of Geldart B group) and assuming an average Courant number of 0.15, a cell face size of 1.0 cm and a gas velocity of 2 m/s, then the recommended time step would be  $\Delta t=0.00075$  s. Using this value as a rough guide, the choice has been made here to start the simulation with a step size of 0.0005 s. This was then increased to 0.001 s for the rest of the simulation once the first few seconds converges. While this proved successful in avoiding computational difficulties and stiffness of the solution at the start, it also allowed a significant reduction in the computational time without jeopardizing the solution accuracy.

In specifying the boundary conditions, the bottom of the riser and solid inlet were set at a fixed air velocity and fixed solid mass flow rate, respectively. An auxiliary air, specified at a fixed velocity, was set at the solid feeding to create positive pressure, hence, ensuring smooth solid flow and preventing it from backflow. The boundary at the top of the riser was set at atmospheric pressure.

At the wall boundary, the gas phase was set at zero velocity (no-slip condition) while the solid phase is satisfying the widely used boundary conditions:<sup>48</sup>

$$n\tau_{si} \frac{u_{si}}{|u_{si}|} + \frac{\sqrt{3}\pi\phi' g_{oi}\rho_{si}\varepsilon_{si}|u_{si}|\sqrt{\theta_{si}}}{6\varepsilon_{s-\max}} = 0 \quad (26)$$

$$k_{si} \frac{\partial\theta_{si}}{\partial y} = \frac{\sqrt{3}\pi\rho_{si}g_{oi}\varepsilon_{si}\sqrt{\theta_{si}}}{6\varepsilon_{s-\max}\mu_{si}} \left[ \phi'|u_{si}|^2 - \frac{3\theta_{si}}{2}(1-e_{iw}^2) \right] \quad (27)$$

where  $e_{iw}$  is the particle-wall restitution coefficient for solid phase  $i$  and  $\phi'$  is the specular coefficient. The values of these parameters, as well as the values of the other parameters appearing in the model constitutive equations, are given in Table 3.

Initially, the simulation domain was set to atmospheric pressure and the gas and solid phases were introduced at the specified flow conditions. For post-processing and statistical data analysis, the simulation results were sampled every 10 time-steps, but autosaved every 20 time-steps to avoid unnecessary data storage. The steady state flow condition was achieved after around 10 s of real-time simulation (corresponds to around 24 hrs of CPU time). The time-averaged steady state data was calculated after excluding the first 5 seconds.

## 5. Results and discussion

### 5.1. Model sensitivity analysis

Before going into the model validity, it is important first to establish the conditions required to achieve solution independent of grid size and time step. It is also important to assess the various option of constitutive equations as well as to identify the best solution procedure for economic computational time and reliable results.

### 5.1.1. Cell size and time step

Fig. 5 shows the predicted solid concentration profile computed using three different solution time steps. The results produced using a time step of 0.1 s clearly deviate from the rest, particularly near the wall region. This is not surprising since the relatively dense wall layer is a major source of turbulence due to the expected large velocity and pressure gradients. This essentially requires refined time step to resolve. The default time step of 0.001 s, which was decided earlier based on the Courant number, appear to produce results closely matching that produced at a time step of 0.01 s. Accordingly, all the results shown in this study were produced using a time step of 0.001 s, unless otherwise stated.

Several different cell sizes have been investigated to show the model sensitivity and confirm the appropriate cell or element numbers for the current simulation. This is demonstrated in terms of the velocity profiles of the wood particles at a selected operating condition as shown in Fig. 6. The results were produced with varying the number of cells through changing the upper and lower face size limits. With the exception of the finer cell size (total cells number of 69433), all of the other settings appear to show similar profiles with negligible numerical differences. The observed deviation at the finer cell is due to the fact that the specified lower face limit, which is 0.5, falls below the minimum required size (i.e. 10 times the larger particle size in the binary mixture), therefore, the model failed to correctly resolve the flow structure relevant to this particle size. Accordingly, in order to satisfy a solution independent of the cell size for a polydisperse mixture the recommended rule of thumb is:

$$\text{cell face size} \geq 10 d_{s,max}. \quad (28)$$

where  $d_{s,max}$  is the diameter of the larger particle in the mixture.

### 5.2.1. The solution of the energy equation

The granular temperature is an important parameter required for the description of the solid phase stresses. In the context of Eulerian-Eulerian modeling, the granular temperature represents the solid phase kinetic energy fluctuation due to the random motion of particles. As discussed in Section 3.1, the model can be solved by using the full partial differential equation (PDE) of the kinetic energy (Eq. 6) or by using its simplified algebraic version (Eq. 7), which neglects the convection and diffusion terms. In terms of the solution stability and computation time, the experience has shown that the algebraic equation produces a stable solution at a reasonable computational time step. This is simply because the energy equation, in this case, is solved in a single step (i.e. non-iterative solution). On the other hand, the full kinetic energy for a binary mixture is stiff and the solution requires setting a relatively small time step to avoid instability and complicated divergence problem, which, in turn, results in increasing the computational time. In modeling of a CFB reactor with multi-solid phases and added complexity of reactions and heat transfer, it is important to seek methods to minimize the computational time.

To start with, Fig. 7 compares the predicted average granular temperature profile along the riser height for a monodispersed system (single solid phase). Here, it is clear that both options produce similar results with negligible numerical differences, although with much less computational time in the case of algebraic solution option. This suggests that the kinetic energy dissipate locally, hence the contributions of convection and diffusion kinetic energies may be omitted in modeling a CFB without critically losing the main hydrodynamic features of the flow. The solution of the

model for a binary solid mixture using the full energy equation (Eq. 6) has been found to be very sensitive to the solution time-step, such that convergence can only be achieved at a very small time step, and in many cases the solution fails even at a very small time step of  $10^{-6}$  s.

Fig. 8 shows the predicted cross-sectional average granular temperature and the corresponding solid concentration profiles for the two dispersed solid phases along the riser height. The larger particle of 755  $\mu\text{m}$  is at higher concentration and higher granular temperature than the smaller particle of 360  $\mu\text{m}$ . This suggests that the simplified energy equation is capable of predicting physically sound trends since, within the dilute regime, the granular temperature is proportional to the solid concentration<sup>49</sup> ( $\theta \propto \varepsilon_s^{2/3}$ ). Quantitatively, the values of the granular temperature obtained here are close to the data reported for Geldart Group B particles in a CFB riser<sup>49</sup>, hence giving more confidence on the adopted solution of the energy equation.

### 5.1.2. Turbulence

Fig. 9a shows the predicted pressure profile across the riser height with and without incorporating the dispersed RNG  $k$ - $\varepsilon$  turbulence model. The result clearly shows the model to be very sensitive to the turbulence. This is expected since the turbulence transfer among the phases in a binary mixture plays a more dominant role especially when there are rapidly strained flows and swirl effects. Fig. 9b shows the variation of the solid velocity at the solid entrance region. This due to the entrance effect associated with the introduction of a high solid flux from one side of the reactor assisted with a secondary airflow to create positive pressure at the entrance point. This appears to cause high downfall velocity and non-uniform velocity distribution, which, in turn, causes significant turbulence that, propagates towards the top parts of the reactor. The work of Hartge et

al.<sup>51</sup> on modeling of turbulence in CFB (dilute suspension) and that of Wang et al.<sup>52</sup> on bubbling bed (dense suspension), have both shown that the dispersed RNG  $k-\varepsilon$  model produces improved predictions, hence confirming its applicability to wider flow regimes. In the rest of this study, the turbulence model will be used as default unless otherwise stated.

### 5.1.3. Constitutive equations

#### 5.1.3.1. Solid-gas momentum exchange coefficient (gas drag)

Fig. 10 shows the predicted pressure profiles along the riser height using the two solid-gas momentum exchange equations proposed by Gidaspow<sup>30</sup> and Syamlal et al.<sup>33</sup>, as given in Section 3.2.1. The simulations were carried out using single solid phases, each of different particle size and flow conditions. The profiles on the left side of Fig. 10 are for a small particle size at dilute circulation, while the ones in the right are for a relatively larger particle size and denser circulation. It is clear that both models produce comparable results at the dilute condition. In the denser condition, the differences become well pronounced. This suggests that these drag models behave differently with increasing solid concentration. This discrepancy is understood to arise from the fact that Gidaspow's model switches between two different drag models at the solid volume fraction 0.2, while Syamlal's model has the advantage of being continuous over a wide range of solid concentration. Moreover, Almuttahir<sup>27</sup> suggested that Syamlal model is of better predictive capability for the range of operating conditions used in CFB risers. In the rest of this study, the solid-gas momentum exchange coefficient of Syamlal (Eq. 13) will be used as default unless otherwise stated. The validity of this choice for a binary mixture will be demonstrated in Section 5.3 when comparing the model predictions with the experimental measurements.

### 5.1.3.2. Solid-solid momentum exchange coefficient

Fig. 11 shows a comparison between the predicted pressure profile with and without solid-solid momentum exchange for a binary mixture. The results confirm the critical sensitivity of the solution to this parameter, particularly at the bottom of the riser where the solid concentration is high and the velocity difference between the two solid phases is significant. This is interesting, since there is a general understanding that the momentum exchange between the solid phases in a polydispersed dilute suspension, such as in CFBs, is negligible, especially if the solid phases are of limited size and density differences. In a biomass gasifier, the physical differences between the solid phases (e.g. wood particles and sand) is high, therefore, the incorporation of the solid-solid momentum exchange in the hydrodynamic model becomes essential. It is worth noting that Yin and Sundaresan<sup>53,54</sup> and Holloway et al.<sup>55</sup>, using Lattice-Boltzmann simulations, reported similar conclusion, though in different ranges of particle sizes, mixing ratios and Reynolds number than the ones considered here.

### 5.1.3.3. Radial distribution function and solid pressure

The radial distribution function appears in various constitutive equations, as noted earlier, among which, is the solid pressure (Eq. 22). It is of interest here to quantify and assess the degree of the model sensitivity and deviations when applying any of the three radial distribution functions given earlier in Section 3.2.2. This is less understood and rarely discussed in the literature for a binary solid mixture of considerable physical differences. Fig. 12 shows the variations of the radial distribution function and the solid pressure for a binary solid mixture as a function of the total solid concentration. The values calculated by Syamlal<sup>33</sup> and the modified Bagnold<sup>21</sup> models are clearly very close, however, both models behave differently at the high concentration near the maximum

packing. On the other hand, the modified Bagnold<sup>21</sup> and Iddir and Arastoopour<sup>43</sup> models both appear to correctly increase exponentially towards infinity as the solid concentration approached maximum packing.

In a dilute suspension, the impact of the solid pressure on the overall flow hydrodynamic is limited (i.e. the pressure term appearing in the solid momentum equation, Eq. 5, will be factored by a small number). However, it is of interest to here to assess the sensitivity of the solid pressure and the overall hydrodynamic prediction to the employed radial distribution function. Fig. 13 shows the calculated solid pressure as a function of the solid concentration using two different radial distribution functions. The curves trend is in good agreement with the data produced experimentally by Gidaspow et al.<sup>49</sup> and Campbell and Wang<sup>56</sup>. Within the range of low solid concentration relevant to CFB, the solid pressure is dominated by kinetic interactions, while in the high solid concentration this is dominated by collisions. Quantitatively, it is clear that the difference in the computed solid pressure is insignificant, especially within the range of intermediate solid concentration. Therefore, it is concluded that the radial distribution functions of saymala<sup>33</sup> and the modified Bagnold<sup>21</sup> function can both be used in the simulation of the CFB riser with negligible numerical differences. In the rest of this study, the saymala<sup>33</sup> function will be used as the default, unless otherwise specified.

## **5.2. Recommended constitutive and closure equations**

Following the above analysis and based on experience in modeling gas-solid flows, the recommended constitutive and closure equations for modeling the hydrodynamics of a binary solid

mixture in a CFB riser using the Eulerian-Eulerian KTFG model are summarized in Table 4. This model will now be validated against experiment measurement in Section 5.3.

### **5.3. Model validation**

This section shows the results of model validation by comparing the experimental measurements with the hydrodynamic predictions obtained by solving the main model with the recommendations given earlier in Table 4. In addition, this section includes comments on some of the interesting hydrodynamic features of the CFB riser considered. It should be noted that the validation is limited to the range of solid circulation rate, particle size, concentration and velocities commonly used in a fast CFB gasifier. Caution must be exercised if the model is to be used for conditions beyond these regimes.

#### **5.3.1. Pressure profile**

The model validation was first considered by comparing the predicted axial pressure profile with the experimental measurement, as shown in Fig. 14. The profiles show classic feature of CFB risers where the pressure gradually decreasing towards the exit. The calculate mean deviation from the experimental measurements is 1.2% for the curve to the left side of Fig. 14, compared to 4.5% deviation for the curve to the right. The improved accuracy in the first case suggests that the model has better predictive capabilities at the uniform flow of limited velocity and pressure variations. Nevertheless, the deviations in both cases remain considerably small, and therefore, the model predictive capabilities are deemed good enough to reveal the main features of the flow structure in the CFB riser, as further demonstrated here.

### 5.3.2. PEPT measurements and particle dynamic behavior

As described earlier, the PEPT technique applied here is based on tracing a single particle at a time within a given time and space domain. This allows calculating the discrete particle position and velocity. Fig. 15 shows an example of the PEPT detections of a radioactive wood particle in a binary mixture of wood and sand during circulation between the riser and downer sides of the CFB system. The detections show the particle axial position within the lower part of CFB riser. In Fig. 15-a it is clear that there is around 3-6 minutes delay between each detection as the particle circulation completes a full cycle. As a result, there was around 20–40 set of detections in each 2 hours run. Most interesting, Fig. 15-b indicates that the particle dynamic movement in this zone is more complex than it is thought. The particle appears to travel upward and downward and sink in the bottom denser region of the riser as indicated by the gap in signal detection. The corresponding particle velocity is shown in Fig. 16. Here it is shown that the particle accelerates and descend with the velocity ranging between 3 m/s and -2 m/s. This was not an isolated case, but a rather consistent behavior in most of the recorded PEPT data, especially when operating at low fluidization velocity.

Fig. 17 shows the predicted time evolution of the particle concentration within the lower part of the riser. Here, the prediction shows the gradual increase in the solid concentration below the feeding point as the time progresses. This is well resembling the particle dynamics at the bottom of the riser as detected by the PEPT measurement and hence, lending support to the model validity and capability in predicting the experimentally observed behavior. It is believed that the particle circulation in the bottom of the riser relates to the gas swirling and/or increased solid exchange between the dense-wall layer and the core in this region. A similar bottom bed behavior has been previously reported by Grace et al.<sup>2</sup> when experimentally studying the wall-core particle exchange

in a fast fluidized bed reactor. Similarly, Chan et al.<sup>57</sup>, also observed descend of particles near the solid feeding point in a CFB riser by using particle tracking technique. In biomass gasification, such behavior is desirable to enhance the heat exchange between the heat carrier (sand) and the biomass, and hence positively contributes to the rapid thermal decomposition (drying and devolatilization) of the fresh biomass feed at the lower part of the riser.

Fig. 18 shows a comparison between the measured and predicted solid phase velocity at the bottom of the riser. It is recognized that the Eulerian-Eulerian model provides the velocity of the dispersed solid phase while the PEPT data provides the discrete particle velocity. Here, the comparison is made between the time-space averaged axial velocity of the solid phase, determined by the Eulerian-Eulerian model, and the time-space averaged discrete particle velocity within the same space, determined by the PEPT. Clearly, there is good agreement between the measured and predicted velocity. It also observed that the sand particle velocity is low and is less sensitive to the changes in the air velocity compared to the wood. This is due to the fact that the sand is of higher density and is more likely to sink before accelerating towards the top.

### **5.3.3. Granular temperature**

Fig. 19 shows the predicted granular temperatures for a binary solid mixture as a function of the solid volume fraction. This is obtained by recording the predicted granular temperature of each solid phase at a central line extending from the bottom to the top of the riser, thus covering a wide range of solid concentration.

The predicted values of granular temperature, as well as the curve trend, is in agreement with the published data for the particle size range considered. For example, the extensive work by Gidaspow and co-workers<sup>18,20,49,50</sup> on fluidized bed reactors has shown the granular temperature of particle class Geldart B to fall within the range of 0.0001–0.5 m<sup>2</sup>/s<sup>2</sup>. It is interesting to note the increase in granular temperature as the solid concentration increases towards ~0.1, which then decreases as the concentration approaches the maximum packing condition. Within the range of low solid volume fraction below ~0.1, which is commonly classified as kinetic flow regime, the effect of increasing solid concentration on the granular temperature is similar to the effect of compression on gas temperature, i.e. giving the proportional relation  $\theta_s \propto \varepsilon_s^{2/3}$ . This is in good agreement with the data reported by Gidaspow<sup>30</sup> for dilute flow. On the other hand, the decrease in the granular temperature at increasing solid concentration beyond ~0.1 is attributed to the decrease in mean free path due to high solid collisions, this gives the inversely proportional relation  $\theta_s \propto \varepsilon_s^{-2}$ , as reported by Gidaspow<sup>30</sup> for collisional flow. At the other extreme end near to maximum packing (not covered in this study), the granular temperature correctly approach zero.

In summary, there is evidence of good agreement between the prediction and the reported data on granular temperature. Hence, the solution of the granular energy equation using the simplified algebraic alternative offers a reliable approach for the simulation of a polydisperse mixture in a CFB gasifier.

## Conclusions

This study presented a multi-fluid (Eulerian-Eulerian) model of a binary mixture of polydisperse particles in a CFB riser. The study was mainly focused on identifying the appropriate

constitutive/closure equations and solution procedure with the ultimate goal of developing a reliable tool for the simulation of biomass gasification in a CFB system. The model was solved using ANSYS FLUENT Computational Fluid Dynamic (CFD) software.

The model sensitivity to the various options of constitutive equations and alternative method for the solution of the kinetic energy equation has been assessed. The model was found to be highly sensitive to the effect of solid-solid momentum exchange (drag) but less sensitive to the various options of radial distribution functions investigated. The inclusion of a turbulence model proved to be crucially impotent for accurate predictions and resemblance of the experimentally observed solid recirculation and swirl near the solid entrance at the bottom of the reactor. The two different solution methods of the energy equation, i.e. full PDE and simplified algebraic equation, both produced similar results with the latter being much easier to converge with the added advantage of reduced computational time. Accordingly, a complete hydrodynamic model has been recommended and validated against experimental data. In summary, the model proved to be robust and accurate in predicting the hydrodynamic features of polydispersed particles (binary mixture) in a CFB riser.

### **Acknowledgment**

The authors would like to thank the staff at the University of Birmingham Nuclear Physics Research Group, with special thanks to Prof David Parker, for the support and provision of access to their Positron Emission Particle Tracking (PEPT) system.

## References

- (1) Worley M. and J. Yale. Biomass Gasification Technology Assessment, Consolidated Report, Harris Group Inc. Atlanta, Georgia, 2012.
- (2) Juhui C.; Yin Weijie; Wang Shuai; Yu Guangbin; Li Jiuru; Hu Ting; Lin Feng. Modelling of coal/biomass co-gasification in internal circulating fluidized bed using kinetic theory of granular mixture. *Energy Conversion and Management* 2017, 148 506–516.
- (3) Bashir, M.; Yu, X.; Hassan, M.; Makkawi, Y. Modelling and performance analysis of biomass fast pyrolysis in a solar-thermal reactor. *ACS Sustainable Chem. Eng.* 2017, 5, 3795–3807.
- (4) Lia, X. T.; Gracea, J. R.; Lima, C. J.; Watkinsona, A. P.; Chenb, H. P.; Kim, J. R. Biomass gasification in a circulating fluidized bed. *Biomass and Bioenergy* 2004, 26, 171–193.
- (5) Parthasarathy, P.; Narayanan, K. S. Hydrogen production from steam gasification of biomass: Influence of process parameters on hydrogen yield- A review. *Renewable Energy* 2014, 66, 570-579.
- (6) Wei L.; Xu S.; Zhang L.; Liu C.; Zhu H.; Liu S. Steam gasification of biomass for hydrogen-rich gas in a free-fall reactor. *Int J Hydrogen Energy* 2007, 32, 24–31.
- (7) Ku X.; Tian Li; Terese Lovas. CFD–DEM simulation of biomass gasification with steam in a fluidized bed reactor. *Chemical Engineering Science* 2015, 122, 270–283.

- (8) Gel A.; Shahnam, M.; Musser J.; Subramaniyan, A. K.; Dietiker, Jean-Francois. Nonintrusive Uncertainty Quantification of Computational Fluid Dynamics Simulations of a Bench-Scale Fluidized-Bed Gasifier. *Ind. Eng. Chem. Res.* 2016, 55, 12477–12490.
- (9) Anil M.; Rupesh, S.; Muraleedharan, C.; Arun, P. Performance Evaluation of Fluidised Bed Biomass Gasifier Using CFD. *Energy Procedia* 2016, 90, 154–162.
- (10) Yan L.; Lim, C. J.; Yue, G.; He, B.; Grace, J. R. Simulation of biomass-steam gasification in fluidized bed reactors: Model setup, comparisons and preliminary predictions. *Bioresource Tech* 2016, 221, 625–635.
- (11) Kraft S.; Kirnbauer, F.; Hofbauer, H. CPFD simulations of an industrial-sized dual fluidized bed steam gasification system of biomass with 8 MW fuel input. *Applied Energy* 2017, 190, 408–420.
- (12) Liu H.; Cattolica, R. J.; Seiser, R. CFD studies on biomass gasification in a pilot-scale dual fluidized-bed system, *International Journal of Hydrogen Energy* 2016, 41, 11974–11989.
- (13) Liu H.; Cattolica, R. J.; Seiser, R. Operating parameter effects on the solids circulation rate in the CFD simulation of a dual fluidized-bed gasification system. *Chemical Engineering Science*, 2017, 169, 235–245.

- (14) Parker, D. J.; Forster, R. N; Fowles, P; Takhar, P. S. Positron emission particle tracking using the new Birmingham positron camera, *Nuclear Instruments and Methods*. A477, 2002, 540–545.
- (15) Parker. D. J.; Broadbent, C. J.; Fowles, P.; Hawkesworth, M. R.; McNei, P. Positron emission particle tracking- a technique for studying flow within engineering equipment, *Nuclear Instruments and Methods in Physics Research Section A: Accelerators, Spectrometers, Detectors and Associated Equipment* 19993, 326, 592–607.
- (16) Seville J. A. single particle view of fluidization. 13th International Conference on Fluidization - New Paradigm in Fluidization Engineering, 2010.
- (17) Seville, J.; Ingram, A.; Fan, X.; Parker, D. J. Positron emission imaging in chemical engineering, in *Advances in Chemical Engineering* 2009, 37 (Li, J, ed.) Elsevier, Amsterdam.
- (18) Gidaspow, D.; Bezburuah, R; Ding, J. Hydrodynamics of Circulating Fluidized Beds, Kinetic Theory Approach. In: Potter, O. E. and Nicklin, D.J., Eds., *Fluidization VII*, Proceedings of the 7<sup>th</sup> Engineering Foundation Conference on Fluidization, Engineering Foundation 1991, New York, 75–82.
- (19) Lun, C. K. K.; Savage, S. B.; Jeffrey, D. J.; Chepurniy, N. Kinetic theories for granular flow: inelastic particles in Couette flow and slightly inelastic particles in a general flow field. *Journal of Fluid Mechanics* 1984,140, 223–256.

- (20) Ding, J.; Gidaspow, D. A bubbling fluidization model using kinetic theory of granular flow. *A.I.Ch.E. Journal* 1990, 36, 523–538.
- (21) ANSYS FLUENT 17.0 Documentation: Theory Guide, 2016.
- (22) Mazzei, L. Eulerian modelling and computational fluid dynamics simulation of mono and polydisperse fluidized suspensions, PhD thesis, University College London, UK, 2008.
- (23) Enwald, H.; Peirano, E.; Almstedt, A.-E. Eulerian two-phase flow theory applied to fluidization, *International Journal of Multiphase Flow* 1996, 22, 21–66.
- (24) Hulme I., Clavelle, E., van der Lee, L., Kantzas, A. CFD Modeling and Validation of Bubble Properties for a Bubbling Fluidized Bed. *Ind. Eng. Chem. Res.* 2005, 44, 4254-4266
- (25) Schneiderbauer, S.; Pirker, S. A Coarse-Grained Two-Fluid Model for Gas-Solid Fluidized Beds. *Journal of Computational Multiphase Flows* 2014, 6, 29–47.
- (26) Lohaa, C.; Chattopadhyay, H.; Chatterjee, P. K. Assessment of drag models in simulating bubbling fluidized bed hydrodynamics. *Chemical Engineering Science* 2012, 75, 400–407.
- (27) Almuttahir A., Taghipour, F. Computational fluid dynamics of high density circulating fluidized bed riser: Study of modeling parameters. *Powder Technology* 2008, 185, 11–23.

- (28) Makkawi, Y. T.; Wright, P. C. The voidage function and effective drag force for fluidized beds. *Chemical Engineering Science*. *Chemical Engineering Science* 2003, 58, 2035–2051.
- (29) Makkawi, Y. T; Ocone, R. Modelling of particle stress at the dilute-intermediate-dense flow regimes: A review. *KONA - Powder Science and Technology* 2005, 23, 49–63.
- (30) Gidaspow, D. *Multiphase Flow and Fluidization*, Boston, MA., Academic Press, 1994.
- (31) Ergun, S., Fluid flow through packed columns. *Chemical Engineering Progress* 1952, 48, 89.
- (32) Wen, C.-Y.; Yu, Y. H. 1966. Mechanics of fluidization. *Chemical Engineering Progress Symposium Series* 62, 100–111.
- (33) Syamlal, M.; Rogers, W.; O'Brien, T. J. 1993. MFIx documentation theory guide. Other Information: PBD: Dec 1993.
- (34) Owoyemi O., Mazzei, L., Lettieri, P. CFD Modeling of Binary-Fluidized Suspensions and Investigation of Role of Particle–Particle Drag on Mixing and Segregation, *AIChE Journal* 2007, 53, 1924–1940.
- (35) Syamlal, M. The particle–particle drag term in a multiparticle model of fluidization. 1987. DOE/MC/21353-2373, NTIS/DE87006500.

- (36) Chapman, S.; Cowling, T. G. *The Mathematical Theory of Non-uniform Gases: An Account of the Kinetic Theory of Viscosity, Thermal Conduction and Diffusion in Gases*. 3<sup>rd</sup> ed, Cambridge Mathematical Library, 1970.
- (37) Halvorsen, B. B. *An Experimental and Computational Study of Bubble Behaviour in Fluidized beds*. PhD thesis, The Norwegian University of Science and Technology (NTNU), 2005.
- (38) Wang S.; Liu, G.; Lu, H.; Yinghua, B.; Ding, J.; Zhao, Y. Prediction of Radial Distribution Function of Particles in a Gas-Solid Fluidized Bed Using Discrete Hard-Sphere Model, *Ind. Eng. Chem. Res.* 2009, 48, 1343–1352.
- (39) Savage, S. B. Streaming motions in a bed of vibrationally fluidized dry granular material. *J. Fluid Mech.* 1988, 194, 457.
- (40) Van Wachem B.; Schouten, J. C.; van den Bleek. C. M. Krishna, Comparative Analysis of CFD Models of Dense Gas–Solid Systems. *AIChE Journal* 2001, 47, 1035–1051.
- (41) Bagnold, R. A. Experiments on a gravity free dispersion of large solid spheres in a Newtonian fluid under shear. *Proc. R. Soc. London* 1954, A225, 49.
- (42) Fedors R.; Landell, R. F. An Empirical Method of Estimating the Void Fraction in Mixtures of Uniform Particles of Different Size. *Powder Technology* 1979, 23, 225–231.

- (43) Iddir, H.; Arastoopour, H. Modeling of multi-type particle flow using the kinetic theory approach. *AICHE Journal* 2005, 51, 1620–1632.
- (44) Lebowitz, J. L. Exact Solution of Generalized Percus-Yevick Equation for a Mixture of Hard Spheres, *Phys. Rev. A* 1964, 133, 895.
- (45) Cornelissen, J. T.; Taghipour, F.; Escudié, R.; Ellis, N.; Grace, J. R. CFD modelling of a liquid-solid fluidized bed. *Chemical Engineering Science* 2007, 62, 6334–6348.
- (46) Gobin, A.; Neau, H.; Simonin, O.; Llinas, J.-R.; Reiling, V.; Selo, J.-L. C. Fluid dynamic numerical simulation of a gas phase polymerization reactor. *International Journal for Numerical Methods in Fluids* 2003, 43, 1199-1220.
- (47) Coroneo, M.; Mazzei, L.; Lettieri, P.; Paglianti, A.; Montante, G. CFD prediction of segregating fluidized bidisperse mixtures of particles differing in size and density in gas-solid fluidized beds, *Chemical Engineering Science* 2011, 66, 2317–2327.
- (48) Johnson, P. C.; Jackson, R. Frictional–collisional constitutive relations for granular materials, with application to plane shearing. *Journal of Fluid Mechanics*, 1987, 176, 67–93.
- (49) Gidaspo D.; Jung, J.; Singh, R. K. Hydrodynamics of fluidization using kinetic theory: an emerging paradigm 2002 Flour-Daniel lecture. *Powder Technology* 2004, 148, 123–141.

(50) Tartan M.; Gidaspow, D. Measurement of granular temperature and stresses in risers, *AIChE* 2004, 1760.

(51) Hartge, E.U.; Ratschow, L.; Wischnewski, R.; Werther, J. CFD-simulation of a circulating fluidized bed riser. *Particuology* 2009, 7, 283–296.

(52) Wang, Q.; Lu, J.; Yin, W.; Yang, H.; Wei, L. Numerical study of gas-solid flow in a coal beneficiation fluidized bed using kinetic theory of granular flow. *Fuel Processing Technology* 2013, 111. 29–41

(53) Yin, X.; Sundaresan, S. Drag Law for Bidisperse Gas–Solid Suspensions Containing Equally Sized Spheres. *Industrial and Engineering Chemistry Research* 2008, 48, 227–241.

(54) Yin, X.; Sundaresan, S. Fluid-particle drag in low-Reynolds-number polydisperse gas-solid suspensions. *AIChE Journal* 2009, 55, 1352–1368.

(55) Holloway W.; Yin, X.; Sundaresan, S. Fluid-Particle Drag in Inertial Polydisperse Gas–Solid Suspensions. *AIChE Journal* 2010, 56, 8, 1194-2004.

(56) Campbell, C. S.; Wang, D. G. A particle pressure transducer suitable for use in gas-fluidized beds. *Meas. Sci. Technol* 1990, 1, 1275–1279.

(57) Chan, C.; Seville, J. P. K.; Baeyens, J. The solids flow in the riser of a CFB viewed by positron emission particle tracking (PEPT). Proceedings of the 13<sup>th</sup> International Conference on Fluidization- New Paradigm in Fluidization Engineering, 2010

ACCEPTED MANUSCRIPT

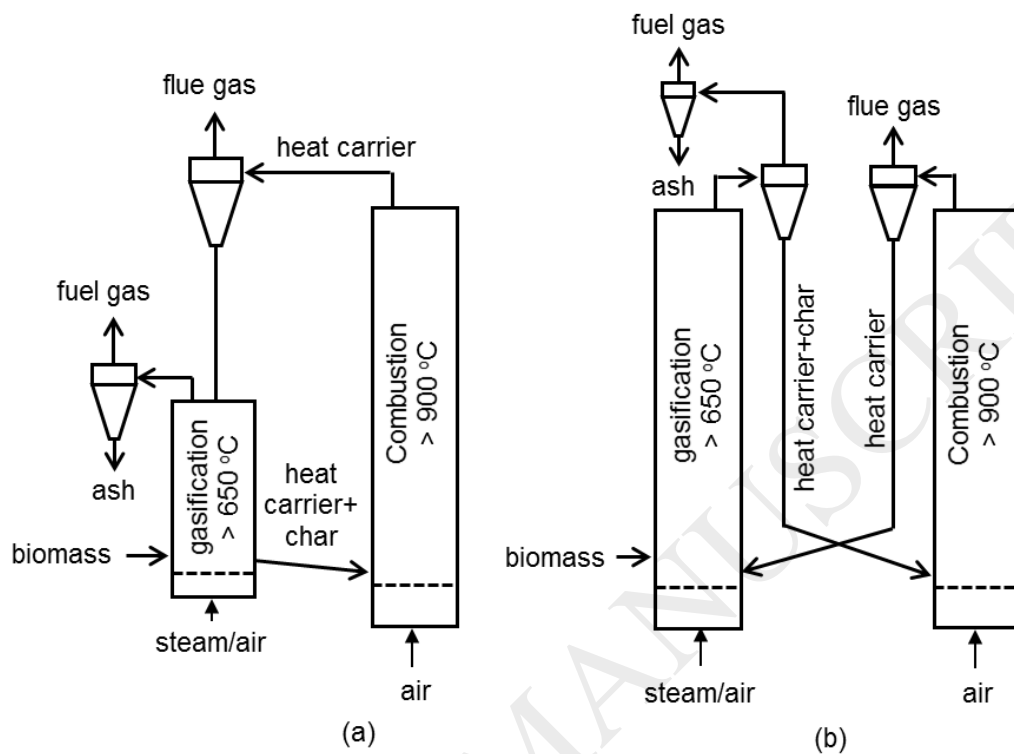


Fig. 1. Examples of dual fluidized bed reactors for biomass gasification (a) bubbling bed coupled with a riser (b) two coupled risers.

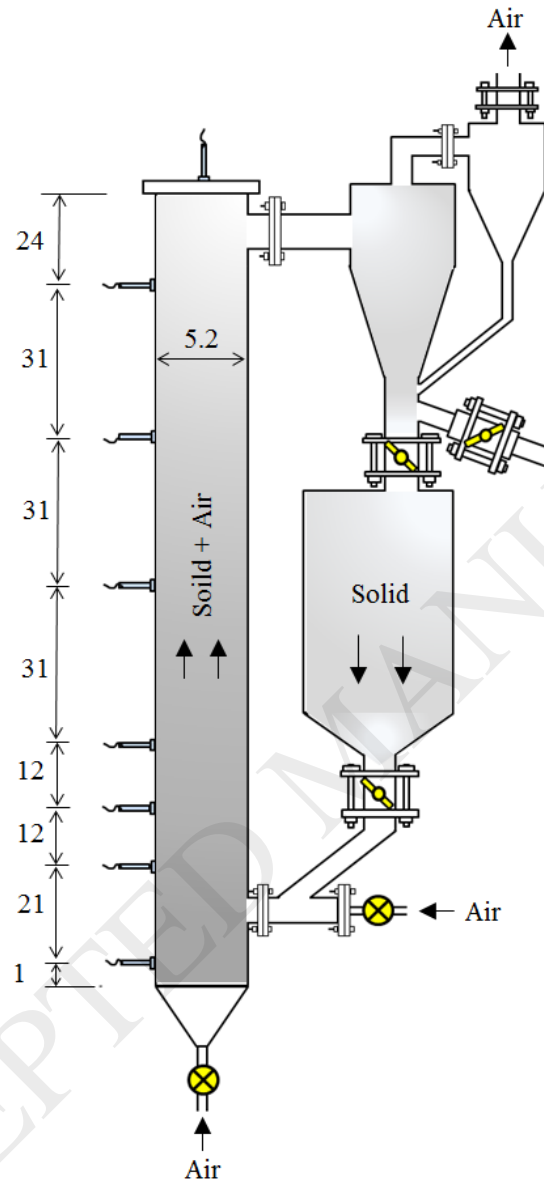


Fig. 2. Schematic representation of the cold flow CFB. All dimensions are in centimeter.

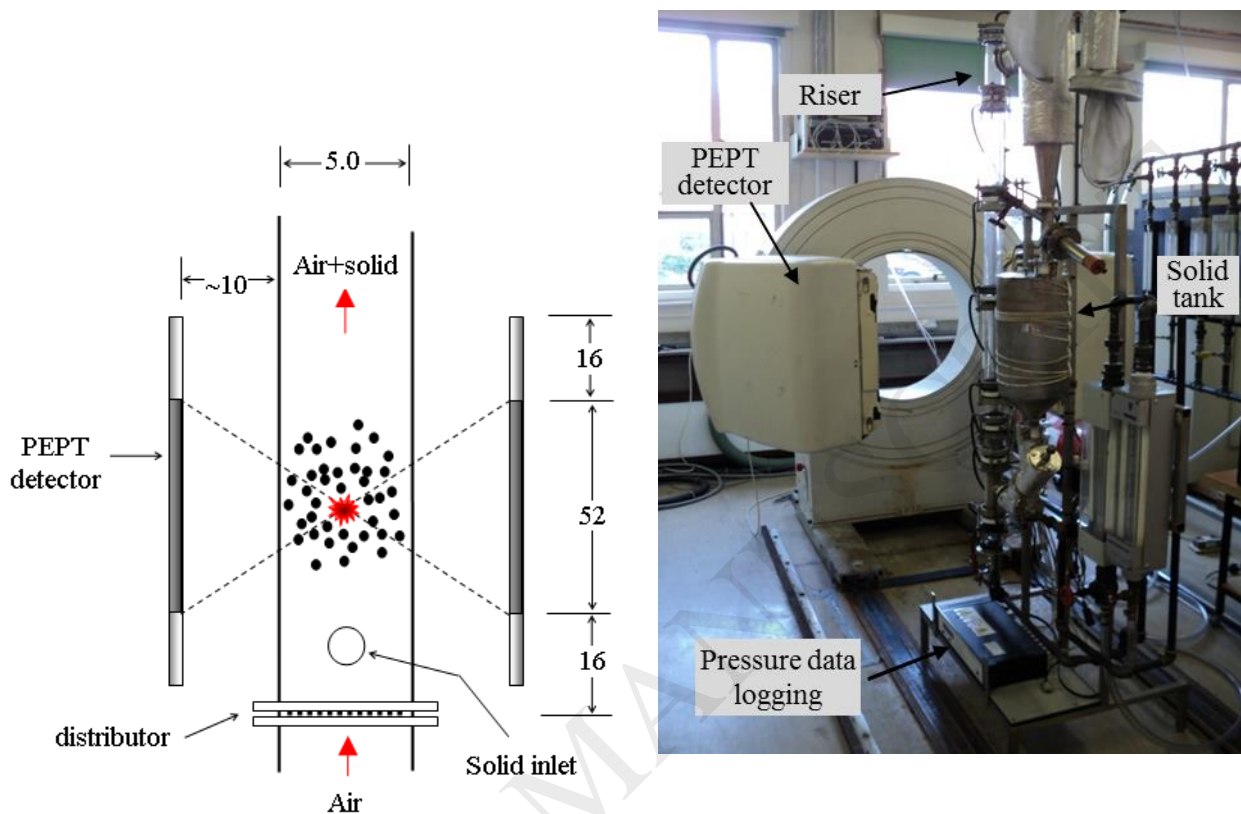


Fig. 3. A schematic description of the PEPT detectors surrounding the lower part of the CFB riser (all dimensions are in cm) and a Photo of the PEPT facility used (Birmingham University, UK).

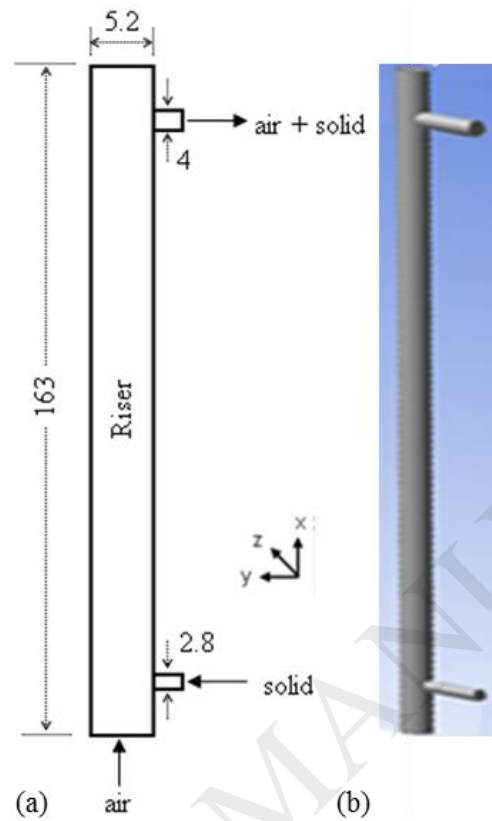


Fig. 4. (a) Schematic representation of the CFB and the simulation domain (b) 3D geometry of the simulation domain generated by ANSYS Workbench software. All the dimensions are in centimetres.

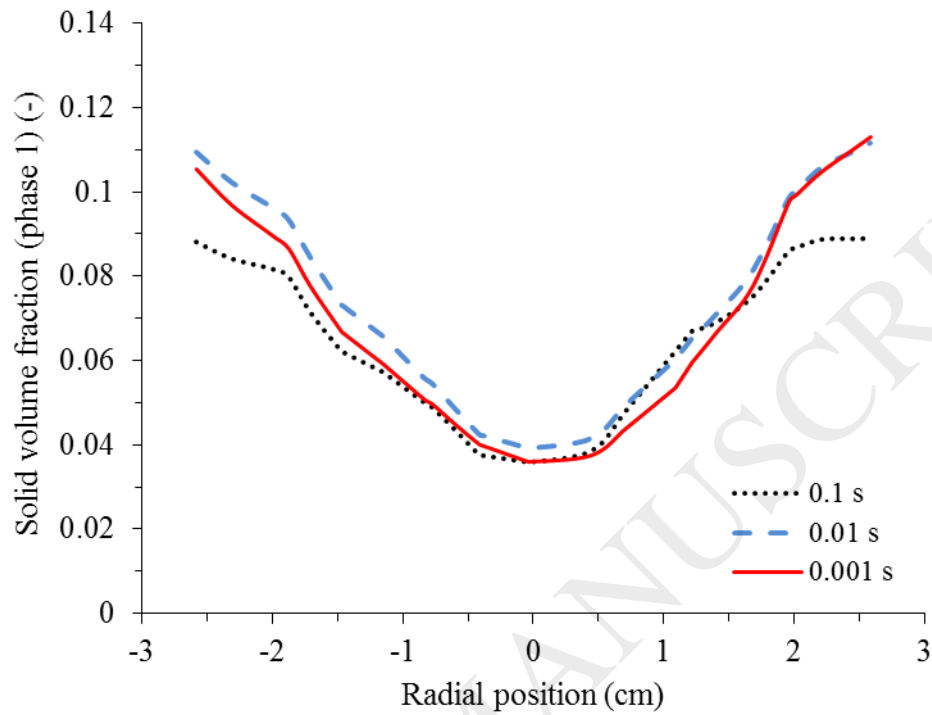


Fig. 5. The solid volume fraction of glass beads at 30 cm above the bottom of the riser demonstrating the model sensitivity to the solution time step. Simulation conditions: a Binary mixture of particles sizes  $d_{s1}=755 \mu\text{m}$  and  $d_{s2}=360 \mu\text{m}$  and equal densities of  $\rho_s = 2500 \text{ kg/m}^3$ , mixed at the ratio of 70:30 wt% respectively and fluidized at the air velocity of 4.6 m/s and a solid circulation rate of 27 g/s.

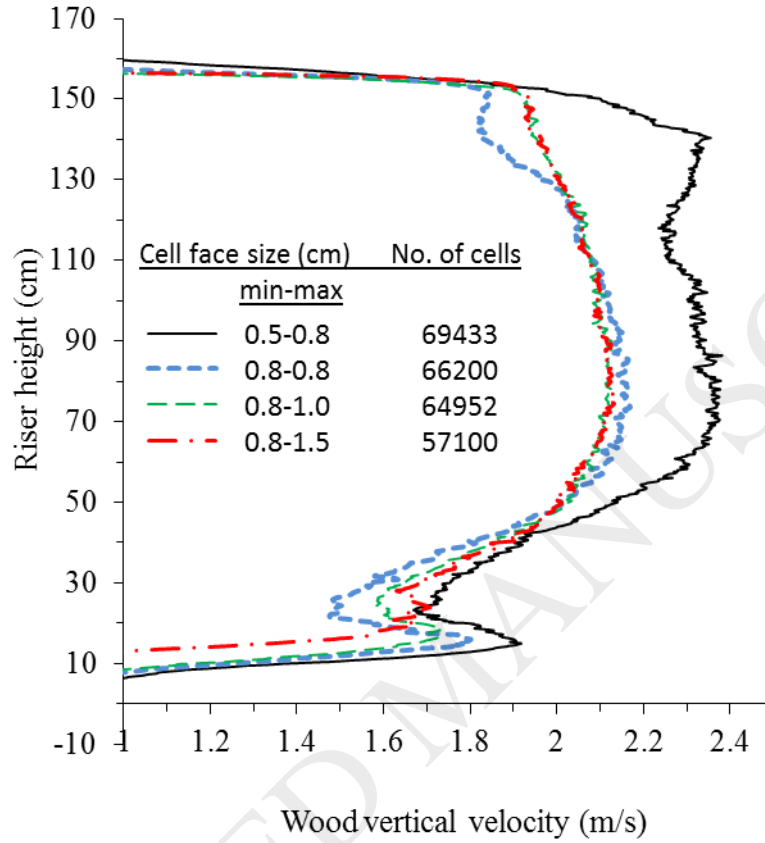


Fig. 6. Vertical velocity profile of the wood particles along the riser height demonstrating the model sensitivity to the cell size. Simulation condition: a Binary mixture of sand ( $d_{s1}=200 \mu\text{m}$ ,  $\rho_{s1}=2600$ ) and wood ( $d_{s2}=500 \mu\text{m}$ ,  $\rho_{s2}=585 \text{ kgm}^{-3}$ ), mixed at the ratio of 70:30 wt%, respectively, and fluidized at the air velocity of 4.6 m/s and a solid circulation rate of 27 g/s.

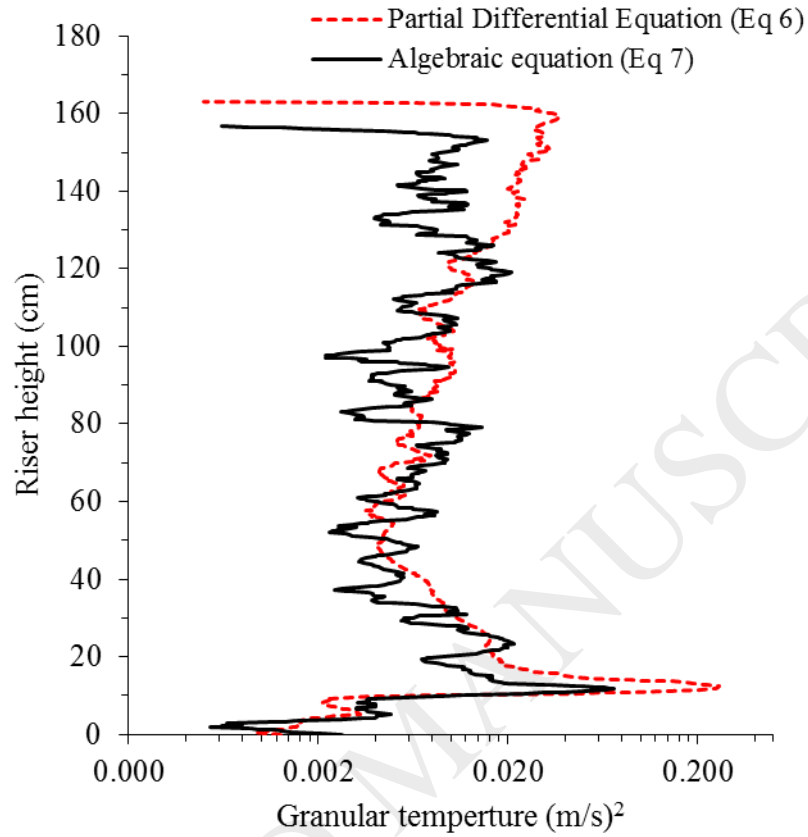


Fig. 7. Comparison of the predicted cross-sectional average granular temperature using two different solutions methods of the kinetic energy equation. Simulation conditions: single solid phase ( $d_s=200\ \mu\text{m}$ ,  $\rho_s=2600$ ) fluidized at the air velocity of 4.7 m/s and solid circulation rate of 36.0 g/s.

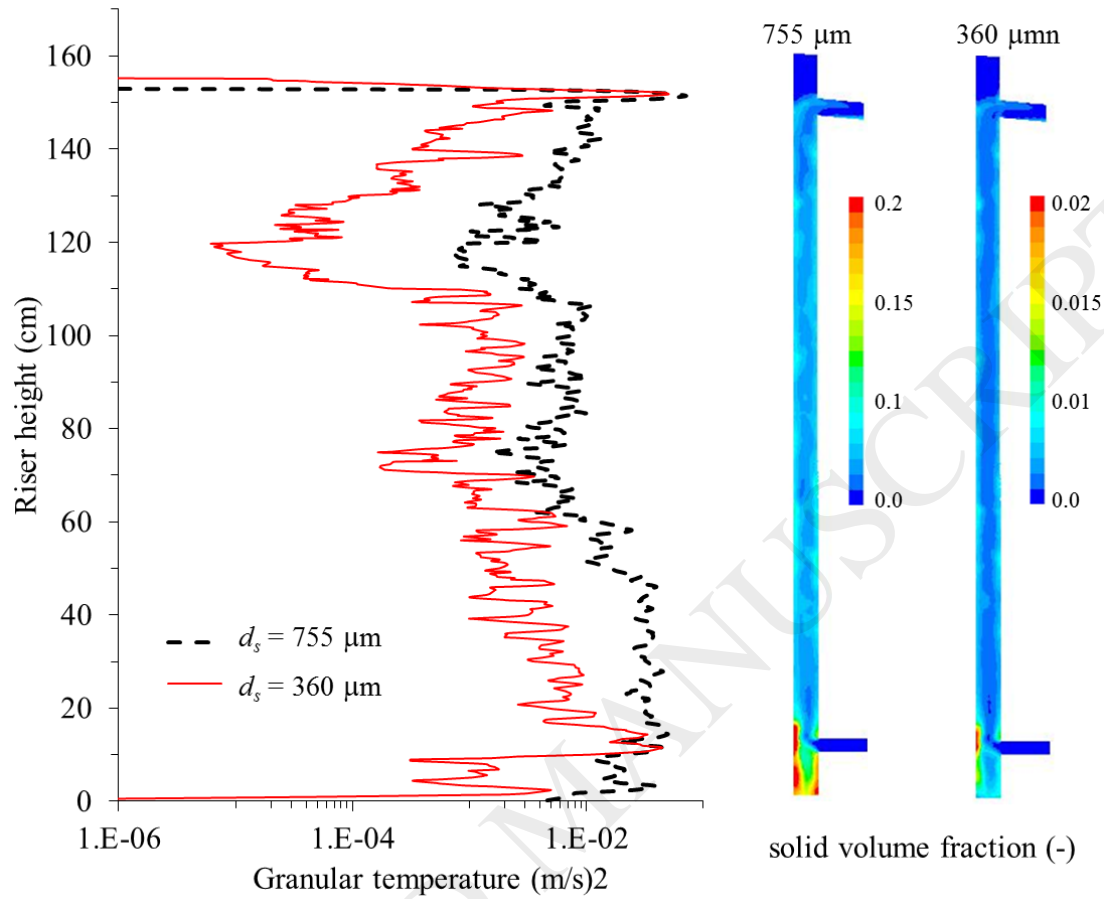


Fig. 8. Predicted average granular temperature and the corresponding solid concentration profiles for a polydispersed binary mixture using the simplified algebraic solution of the energy equation. Simulation conditions: a Binary mixture of particles sizes  $d_s=755 \mu\text{m}$  and  $d_s=360 \mu\text{m}$  of equal densities of  $\rho_s=2500 \text{ kg/m}^3$ , mixed at the ratio of 70:30 wt% respectively, and fluidized at the air velocity of 4.6 m/s and a solid circulation rate of 27 g/s.

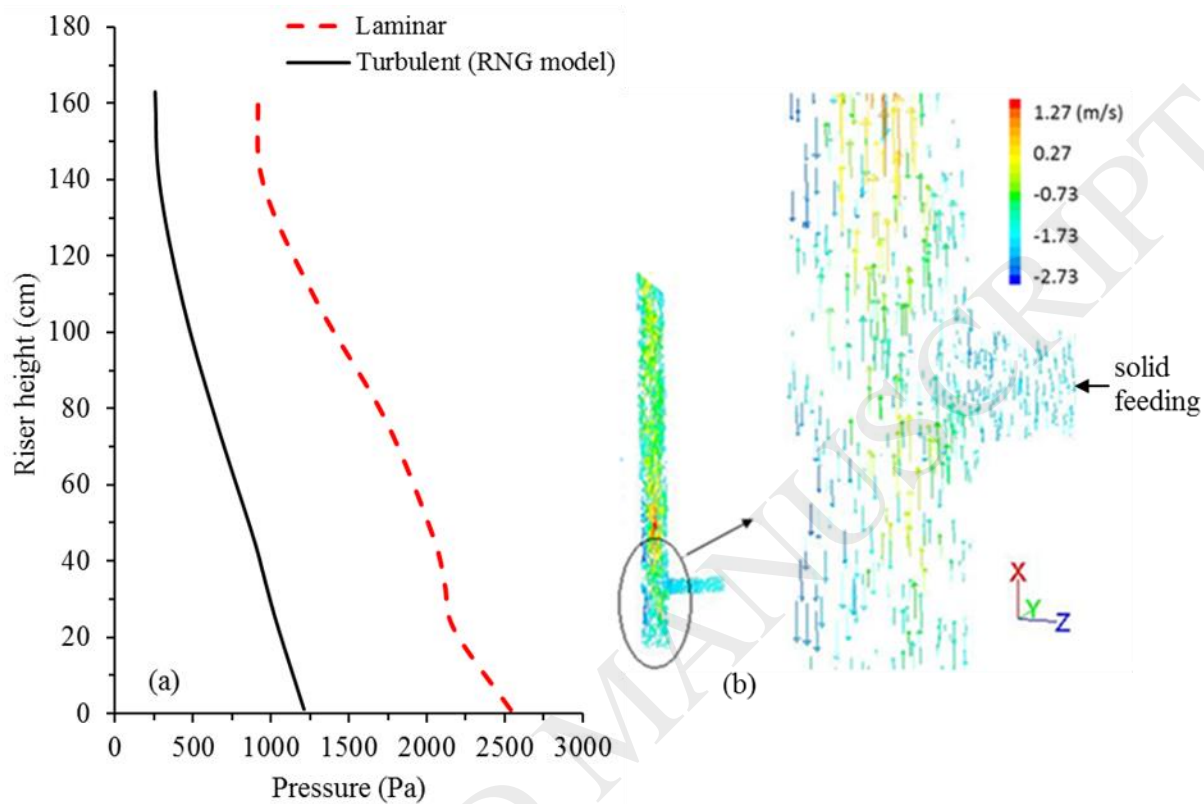


Fig. 9. (a) Comparison of the predicted pressure profile along the riser height demonstrating the effect of turbulence model. (b) contours of the sand velocity vectors at the solid entrance region. Simulation conditions: a Binary mixture of particle sizes  $d_{s1}=400 \mu\text{m}$  and  $d_{s2}=200 \mu\text{m}$  of equal densities of  $\rho_s=2500 \text{ kg/m}^3$ , mixed at the ratio of 70:30 wt% respectively and fluidized at the air velocity of 3.1 m/s and solid circulation rate of 23.0 g/s.

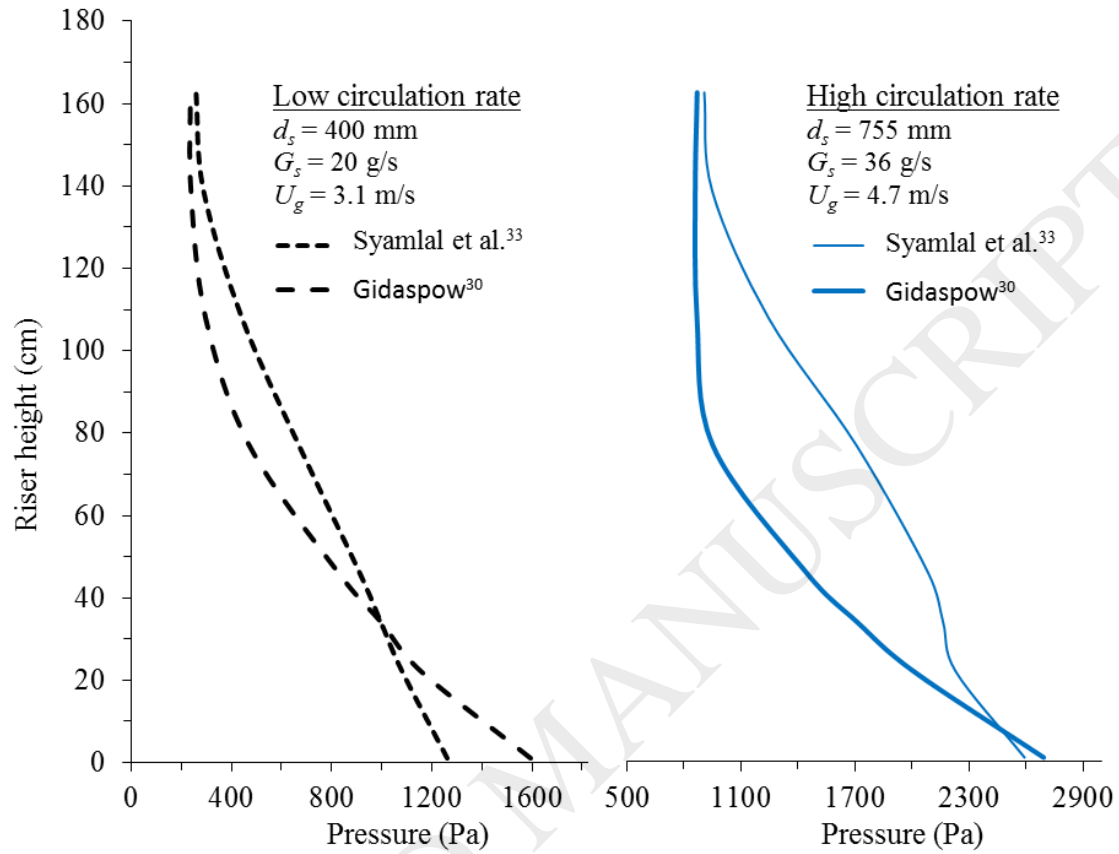


Fig. 10. Comparison of the pressure profiles along the riser height at two different solid circulation rates for a single solid phase predicted by using two different gas-solid momentum exchange models.

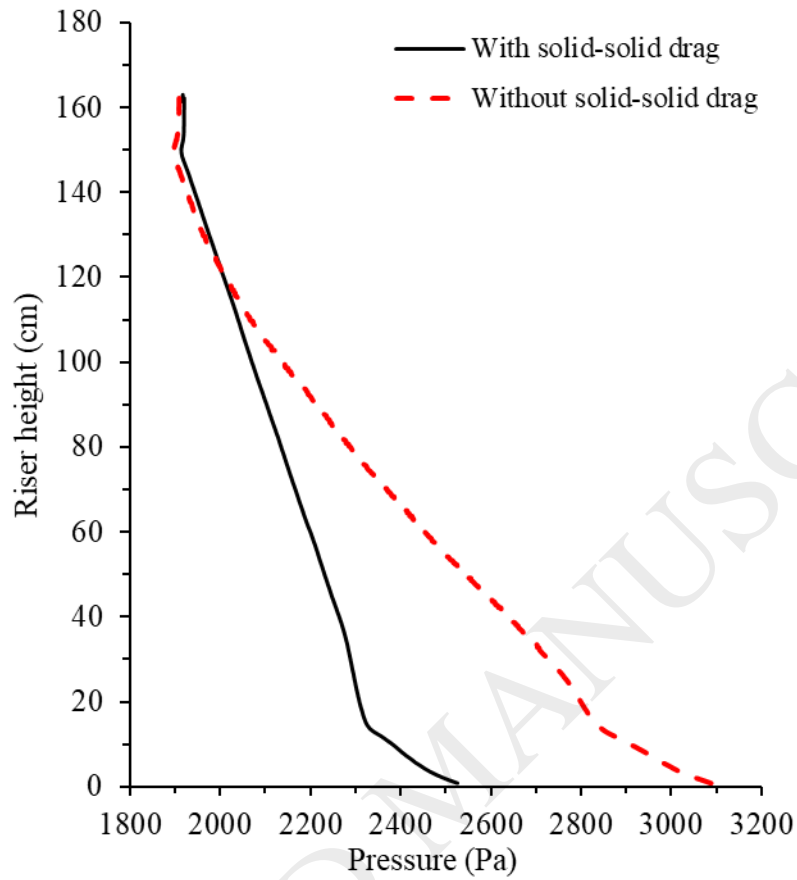


Fig. 11. Comparison of the predicted pressure profile along the riser height demonstrating the model sensitivity to the solid-solid momentum exchange. Simulation condition: Binary mixture of sand ( $d_{s1}= 200 \mu\text{m}$ ,  $\rho_{s1}= 2600$ ) and wood ( $d_{s2}= 500 \mu\text{m}$ ,  $\rho_{s2}= 585 \text{ kgm}^{-3}$ ), at the ratio of 85:15 wt%, respectively, and fluidized at the air velocity of 3.3 m/s and a solid circulation rate of 35 g/s.

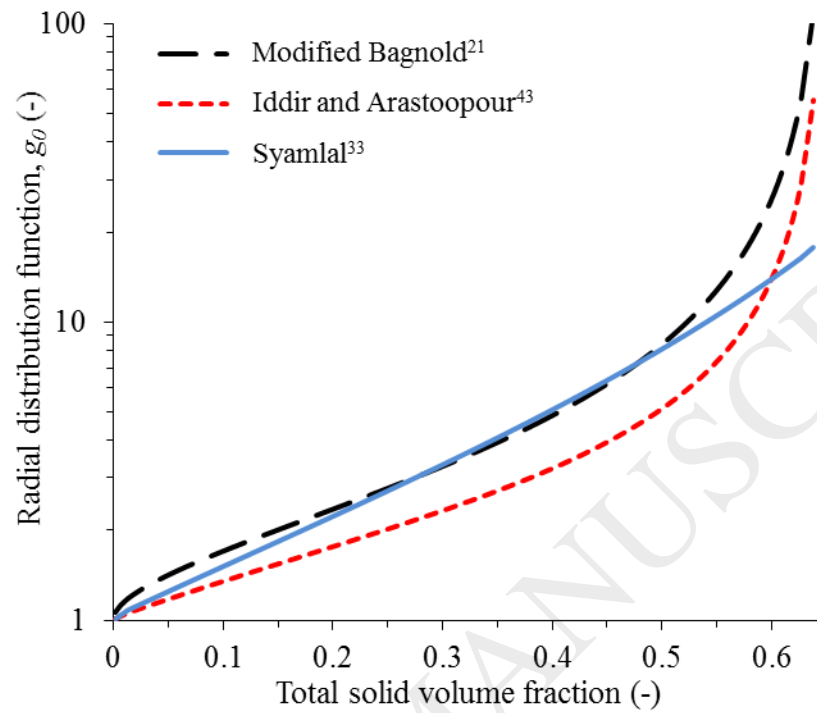


Fig. 12. Comparison of the value of radial distribution functions computed using different alternative functions. Data calculated for a binary solid mixture; particles sizes of  $d_{s1} = 755 \mu\text{m}$  and  $d_{s2} = 400 \mu\text{m}$ , both of density =  $2600 \text{ kg/m}^3$ ; particle-particle restitution coefficient = 0.9.

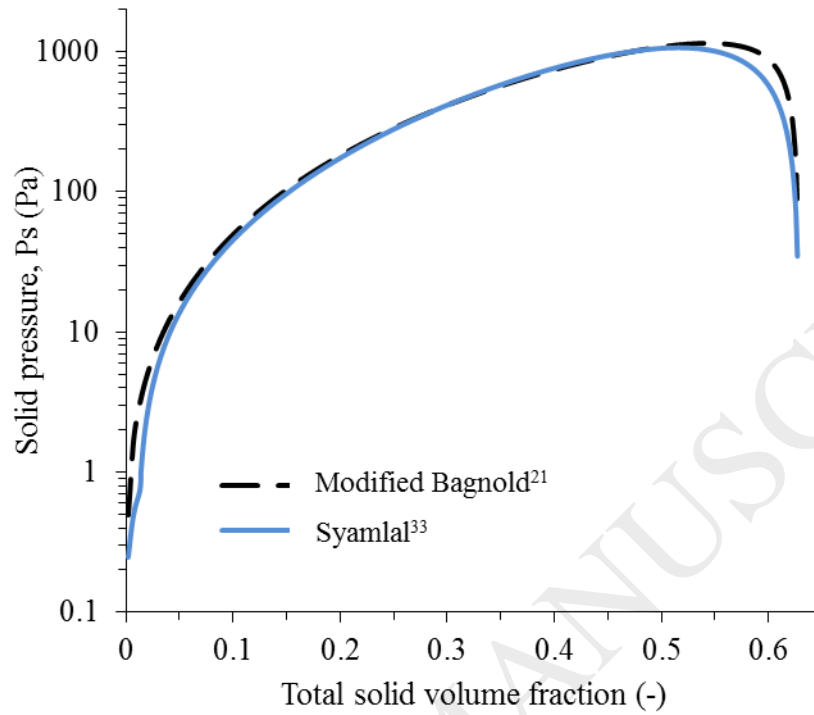


Fig. 13. Comparison of the computed solid pressure using two different radial distribution functions. Data calculated for a binary solid mixture consisting of particles sizes of  $d_{s1} = 755 \mu\text{m}$  and  $d_{s2} = 400 \mu\text{m}$ , both of density  $= 2600 \text{ kg/m}^3$ ; particle-particle restitution coefficient  $= 0.9$ .

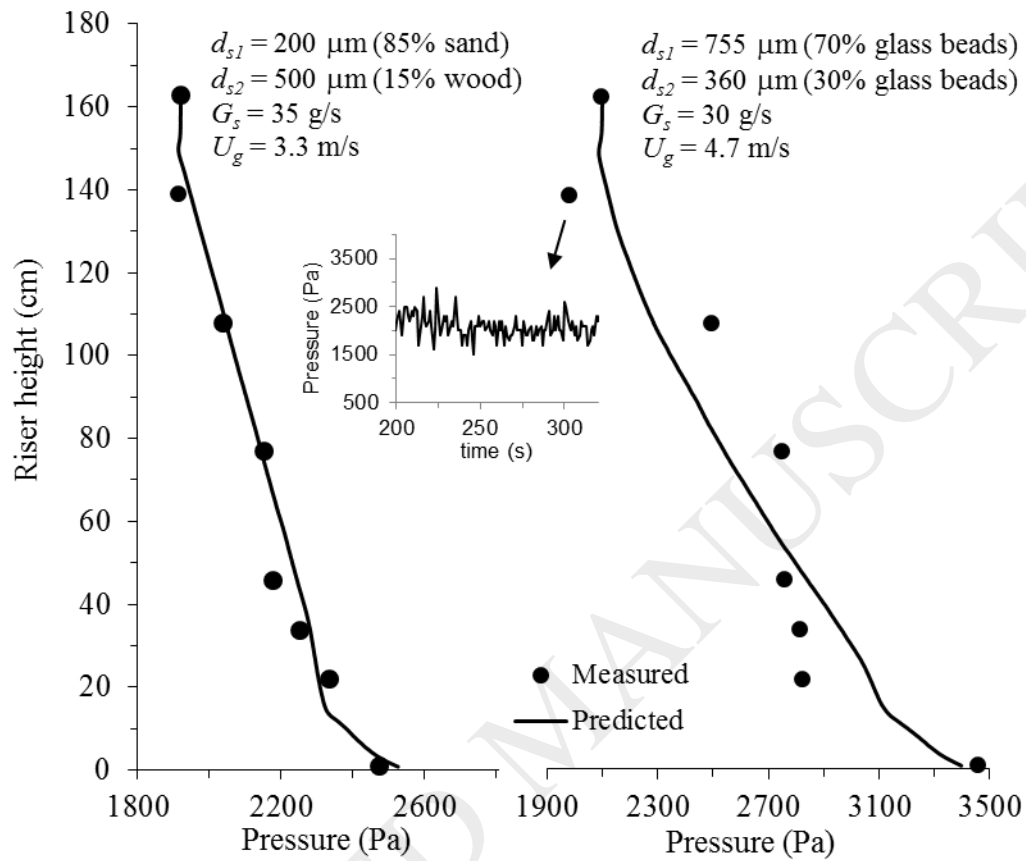


Fig. 14. Comparison of the experimental measurement with the model prediction of the axial pressure distribution in the CFB riser for binary solid mixtures at two different flow conditions.

The inset shows the time series data of the pressure measured at 139 cm.

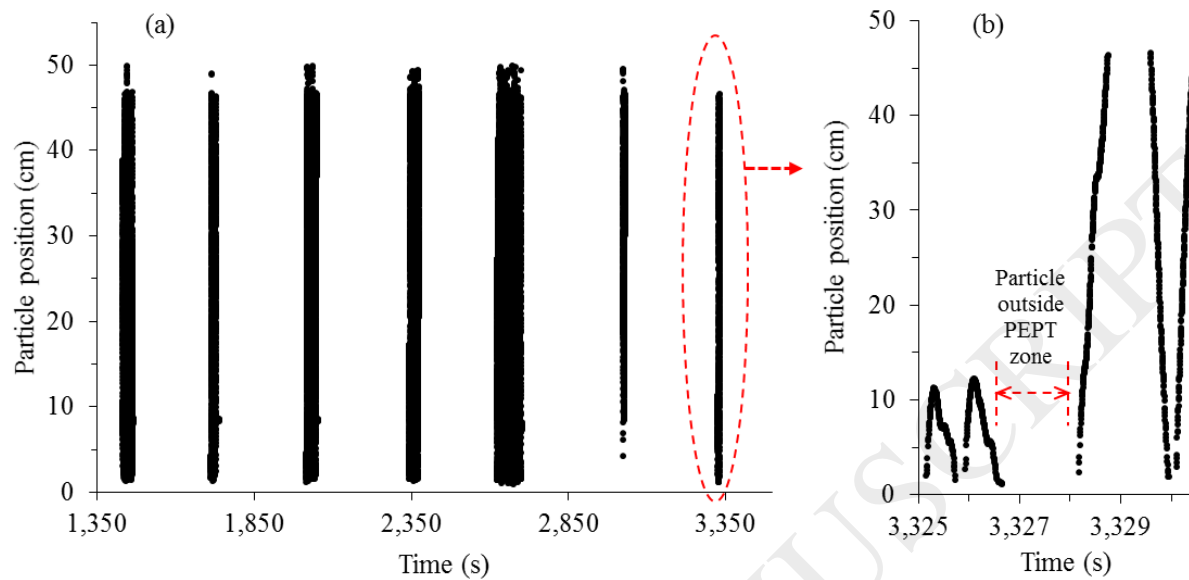


Fig. 15. Example of axial dynamic movement of a radioactive wood particle detected by the PEPT system. Experiment carried out using a mixture of 97% sand ( $d_s = 700 \mu\text{m}$ ,  $\rho_s = 2500 \text{ kg/m}^3$ ) and 3% wood ( $d_s = 1000 \mu\text{m}$ ,  $\rho_s = 585 \text{ kg/m}^3$ ) fluidized at 4.7 m/s and solid circulation rate of 27 g/s.

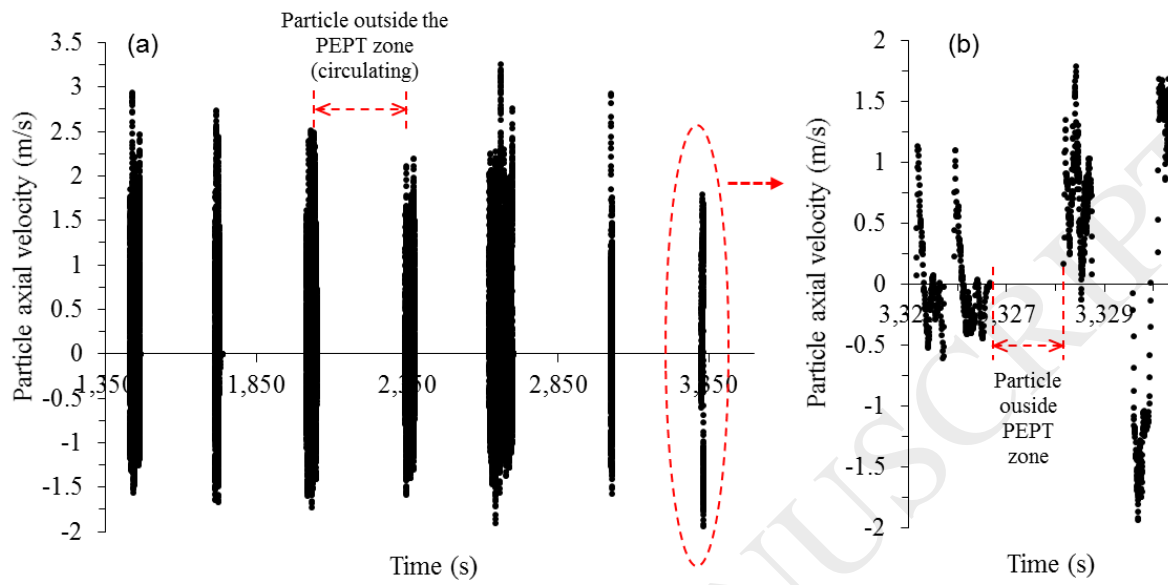


Fig. 16. Example of axial velocity of a radioactive wood particle detected by the PEPT system. Experiment carried out using a binary mixture of 97% sand ( $d_s = 700 \mu\text{m}$ ,  $\rho_s = 2500 \text{ kg/m}^3$ ) and 3% wood ( $d_s = 1000 \mu\text{m}$ ,  $\rho_s = 585 \text{ kg/m}^3$ ) fluidized at 4.7 m/s and solid circulation rate of 27 g/s.

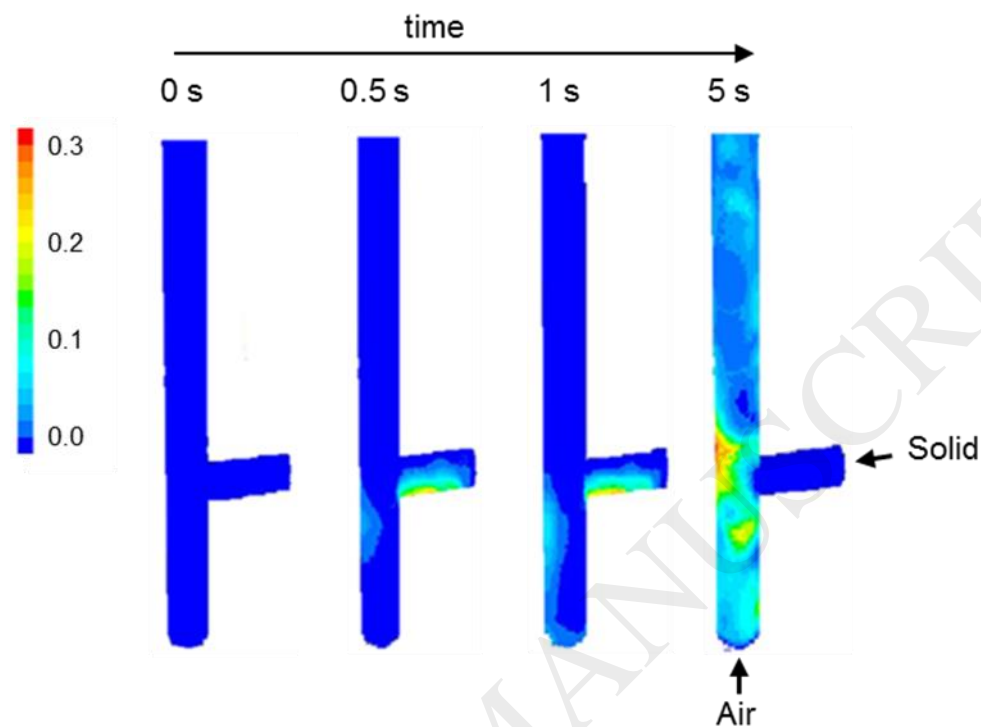


Fig. 17. Contours of the evolution of solid concentration in the lower part of the riser. Simulation condition: binary solid mixture of 97% sand ( $d_s = 700 \mu\text{m}$ ,  $\rho_s = 2500 \text{ kg/m}^3$ ) and 3% wood ( $d_s = 1000 \mu\text{m}$ ,  $\rho_s = 585 \text{ kg/m}^3$ ) fluidized at 4.7 m/s and solid circulation rate of 27 g/s. The color bar represents the range of the solid volume fraction.

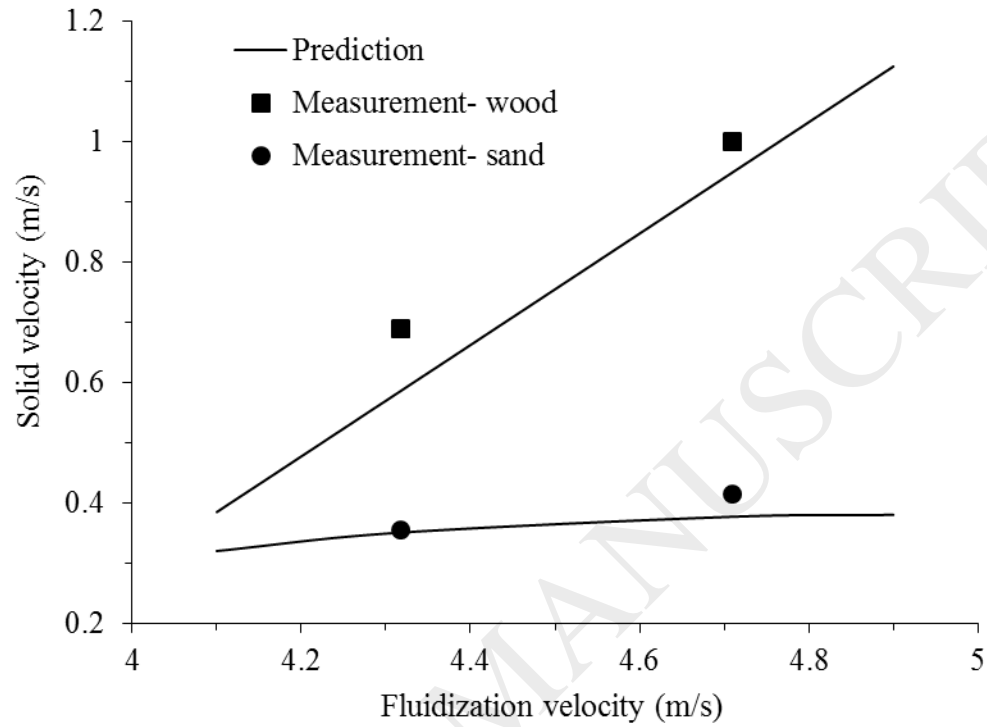


Fig. 18. Comparison between the predicted and measured solid velocity at the entrance region of the CFB for the case of a binary solid mixture of 97% sand ( $d_s = 700 \mu\text{m}$ ,  $\rho_s = 2500 \text{ kg/m}^3$ ) and 3% wood ( $d_s = 1000 \mu\text{m}$ ,  $\rho_s = 585 \text{ kg/m}^3$ ).

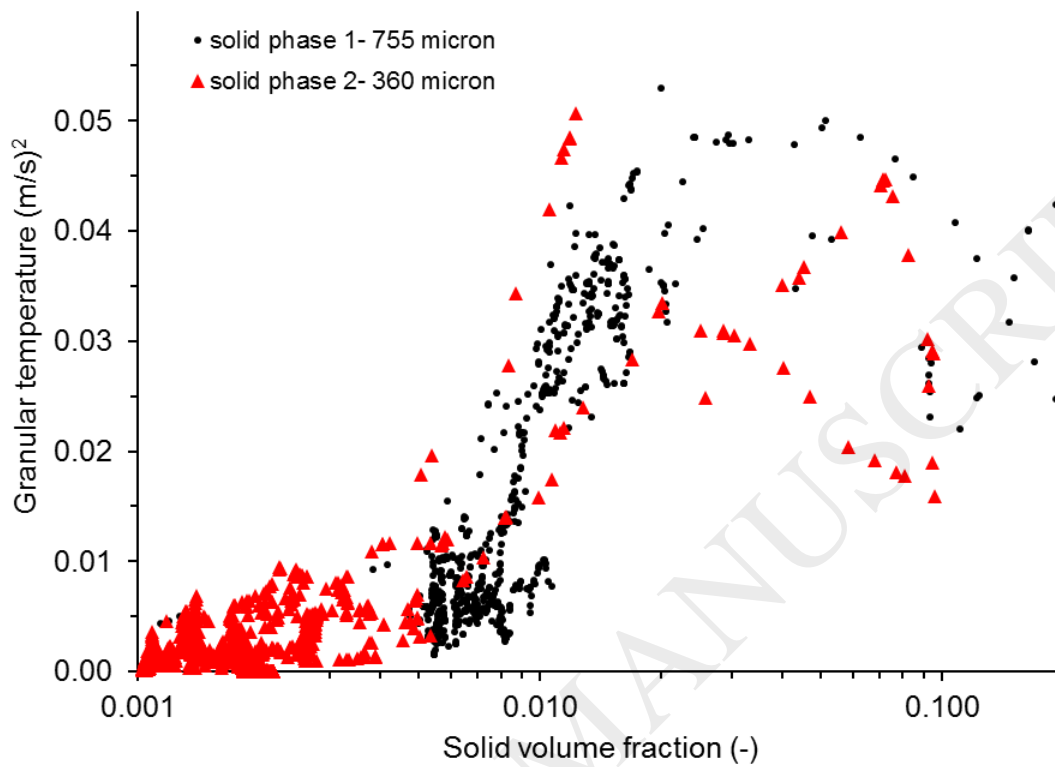


Fig. 19. Predicted granular temperatures for a binary mixture using a simplified algebraic solution of the energy equation. Simulation condition: a Binary mixture of glass beads consisting of 70 wt% of  $d_{s1} = 755 \mu\text{m}$  and 30 wt% of  $d_{s2} = 360 \mu\text{m}$  fluidized at the velocity of 4.6 m/s and a circulation rate of 27 g/s.

Table 1. Summary of some recent studies on modeling of biomass gasification in fluidized bed (FB) reactors

Modeling approach and software	Gasifier type	Main subject of the study	Authors
Model: 3D Eulerian-Lagrangian Software: OpenFOAM	Bubbling FB	<ul style="list-style-type: none"> <li>- Model-set-up</li> <li>- Reactor hydrodynamics and temperature</li> <li>- Effect of steam to biomass ratio</li> <li>- Product gas composition</li> </ul>	Ku et al. <sup>7</sup>
Model: 3D Eulerian-Eulerian Software: MFIX	Bubbling FB	<ul style="list-style-type: none"> <li>- Model sensitivity analysis</li> <li>- Effect of grid resolution</li> <li>- Effect of particle size and steam to biomass ratio</li> <li>- Product gas composition</li> </ul>	Gel et al. <sup>8</sup>
Model: 2D Eulerian-Eulerian Software: ANSYS FLUENT	Bubbling FB	<ul style="list-style-type: none"> <li>- Hydrodynamics and turbulence</li> <li>- Equivalence and steam to biomass ratios</li> <li>- Effect of steam and air temperatures</li> </ul>	Anil et al. <sup>9</sup>
Model: 3D MP-PIC* Software: OpenFOAM	Bubbling FB	<ul style="list-style-type: none"> <li>- Model set-up</li> <li>- Hydrodynamic predictions</li> <li>- Product gas composition</li> </ul>	Yan et al. <sup>10</sup>
Model: 3D MP-PIC* Software: Barracuda	Bubbling FB in a Dual FB system	<ul style="list-style-type: none"> <li>- Steam gasification</li> <li>- Hydrodynamics and temperature distribution</li> <li>- Product gas composition</li> </ul>	Kraft et al. <sup>11</sup>
Model: 2D Eulerian-Eulerian Software: ANSYS FLUENT	Internal circulating FB	<ul style="list-style-type: none"> <li>- Hydrodynamics and reactor temperature</li> <li>- Granular temperature</li> <li>- Product gas composition</li> </ul>	Juhui et al. <sup>2</sup>
Model: 3D MP-PIC* Software: Barracuda	Bubbling FB in a Dual FB system	<ul style="list-style-type: none"> <li>- Hydrodynamics</li> <li>- Solid circulation rate</li> <li>- The impact of gasifier temperature</li> <li>- Effect of steam to biomass ratio</li> <li>- Effect of air supply to the combustor</li> <li>- Product gas composition.</li> </ul>	Liu et al. <sup>12</sup> Liu et al. <sup>13</sup>

\*MP-PIC: Multi-Phase Particle-In-Cell (MP-PIC) is a Lagrangian-based approach.

Table 2. Summary of the experimental unit and range of operating conditions

Experimental unit	
Riser	Diameter= 5 cm; height= 163 cm; material: glass
Solid receiving tank	Cylindrical shape, 1000 m <sup>3</sup> volume; material: steel
Air flow meter	Two rotameters, combined flow of 1900 l/min (max)
Pressure transmitter	0-70 mbar (model CTEM70070GY4)
Cyclones	Main: 47 cm overall height and 12 cm top diameter Secondary: 22.5 cm overall height and 6 cm top diameter
Operating conditions	
Particle sizes and density	Sand: $d = 200 - 700 \mu\text{m}$ ; $\rho_s = 2500 \text{ kg/m}^3$ Wood: $d = 500 - 1000 \mu\text{m}$ ; $\rho_s = 585 \text{ kg/m}^3$ Glass beads: $d_p = 360 - 750 \mu\text{m}$ ; $\rho_s = 2500 \text{ kg/m}^3$
Fluidization velocity	2–5 m/s
Solid circulation rate	40 g/s max (20 kg/m <sup>2</sup> s)
Fluidization medium	Air at ambient condition

Table 3. Values of the fixed parameters used in the solution of the hydrodynamic model

Parameter	Value
Particle-particle restitution coefficient, $e_s$ and $e_w$ (-)*	sand: 0.8 glass beads: 0.9 wood: 0.7
Specularity coefficient, $\phi'$ (-)*	0.5
Maximum solid fraction, $\varepsilon_{s-\max}$ (-)	0.63 (for all solid phases)
Turbulence model constants, $C_1, C_2$ and $C_3$ (-)	1.44, 1.92, 0 (respectively)
Coefficient of friction, $C_{fr}$ (-)	0

\* Values are based on the wide reported literature on fluidization of glass beads, sand and wood particles

Table 4. The recommended constative and closure equations

Gas-solid momentum exchange coefficient <sup>31</sup>	
$\beta_{si} = \frac{3\varepsilon_{si}\varepsilon_g\rho_g}{4u_{r,si}^2 d_{si}} C_D \left( \frac{Re_{si}}{u_{r,si}} \right)  u_{si} - u_g $	$i = 1 \text{ or } 2$
where	
$C_D = \left( 0.63 + \frac{4.8}{\sqrt{Re_{si}/u_{r,si}}} \right)$	
$u_{r,si} = 0.5 \left( \varepsilon_g^{4.14} - 0.06Re_{si} + \sqrt{(0.06Re_{si})^2 + 0.12Re_{si}(1.6\varepsilon_g^{1.28} - \varepsilon_g^{4.14}) + \varepsilon_g^{8.18}} \right)$	
Note: This model is applicable when $\varepsilon_g \leq 0.85$ , otherwise, the term $1.6\varepsilon_g^{1.28}$ should be $2\varepsilon_g^{2.65}$ .	
Solid-solid momentum exchange coefficient <sup>33</sup>	
$K_{ij} = \frac{3(1+e_{ij})\left(\frac{\pi}{2} + \frac{\pi^2}{8} C_{f,ij}\right) \rho_{si} \rho_{sj} \varepsilon_{si} \varepsilon_{sj} (d_{si} + d_{sj})^2 g_{0,ij}}{2\pi(\rho_{si} d_{si}^3 + \rho_{sj} d_{sj}^3)} (u_{si} - u_{sj})$	$i \text{ and } j=1 \text{ or } 2$
where $C_{fr,ls} = 0$ (no friction)	
Granular Viscosity <sup>31</sup>	
$\mu_{si} = \mu_{si,col} + \mu_{si,kin}$	$i = 1 \text{ or } 2$
$\mu_{si,col} = \frac{4}{5} \varepsilon_{si} d_{si} \rho_{si} g_{0i} (1 + e_{si}) \left( \frac{\theta_{si}}{\pi} \right)^{1/2}$	
$\mu_{si,kin} = \frac{\varepsilon_{si} d_{si} \rho_{si} \sqrt{\theta_{si} \pi}}{6(1 - \varepsilon_{si})} \left[ 1 + \frac{2}{5} (1 + e_{si}) (3e_{si} - 1) \varepsilon_{si} g_{0i} \right]$	
Radial distribution function <sup>38,21</sup>	
$g_{0,ij} = \frac{g_{0i} d_{si} + g_{0j} d_{sj}}{d_{si} + d_{sj}}$	$i \text{ and } j = 1 \text{ or } 2$
$g_{0i} = \left[ 1 - \left( \frac{\varepsilon_{s,all}}{\varepsilon_{s,max}} \right)^{1/3} \right]^{-1} + \frac{1}{2} d_{si} \sum_{j=1}^2 \frac{\varepsilon_{sj}}{d_{sj}}$	
where $\varepsilon_{s,all} = \sum_j^2 \varepsilon_{sj}$	
Solids pressure <sup>28,19</sup>	
$P_{si} = \varepsilon_{si} \rho_{si} \theta_{si} + 2\varepsilon_{si} \rho_{si} \theta_{si} \sum_{j=1}^2 \left[ \frac{(d_{si} + d_{sj})}{2d_{si}} \right]^3 (1 + e_{s,ij}) g_{0,ij} \varepsilon_{s,ij}$	$i = 1 \text{ or } 2$
Energy equation	
$0 = \left( -P_{si} \bar{I} + \bar{\tau}_{si} \right) : \nabla u_{si} - \gamma_{si} - 3\beta_{g-si} \theta_{si}$	$i = 1 \text{ or } 2$
Energy dissipation <sup>19</sup>	
$\gamma_{si} = \frac{12(1 - e^2) g_{0i}}{d_i \sqrt{\pi}} \rho_{si} \varepsilon_{si}^2 \theta_{si}^{2/3}$	$i = 1 \text{ or } 2$